Journal of Medicinal Chemistry

pubs.acs.org/jmc

Article

Antitubercular 2-Pyrazolylpyrimidinones: Structure–Activity Relationship and Mode-of-Action Studies

Candice Soares de Melo, Vinayak Singh, Alissa Myrick, Sandile B. Simelane, Dale Taylor, Christel Brunschwig, Nina Lawrence, Dirk Schnappinger, Curtis A. Engelhart, Anuradha Kumar, Tanya Parish, Qin Su, Timothy G. Myers, Helena I. M. Boshoff, Clifton E. Barry, III, Frederick A. Sirgel, Paul D. van Helden, Kirsteen I. Buchanan, Tracy Bayliss, Simon R. Green, Peter C. Ray, Paul G. Wyatt, Gregory S. Basarab, Charles J. Eyermann, Kelly Chibale,* and Sandeep R. Ghorpade*

Cite This: *J. Med. Chem.* 2021, 64, 719–740

Read Online

ACCESS | Metrics & More | Article Recommendations | Supporting Information

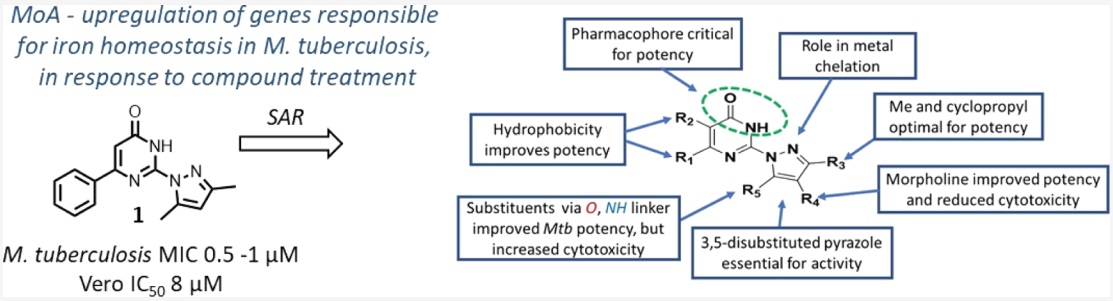

ABSTRACT: Phenotypic screening of a Medicines for Malaria Venture compound library against *Mycobacterium tuberculosis* (*Mtb*) identified a cluster of pan-active 2-pyrazolylpyrimidinones. The biology triage of these actives using various tool strains of *Mtb* suggested a novel mechanism of action. The compounds were bactericidal against replicating *Mtb* and retained potency against clinical isolates of *Mtb*. Although selected MmpL3 mutant strains of *Mtb* showed resistance to these compounds, there was no shift in the minimum inhibitory concentration (MIC) against a mmpL3 hypomorph, suggesting mutations in MmpL3 as a possible resistance mechanism for the compounds but not necessarily as the target. RNA transcriptional profiling and the checkerboard board 2D-MIC assay in the presence of varying concentrations of ferrous salt indicated perturbation of the Fe-homeostasis by the compounds. Structure–activity relationship studies identified potent compounds with good physicochemical properties and *in vitro* microsomal metabolic stability with moderate selectivity over cytotoxicity against mammalian cell lines.

INTRODUCTION

Tuberculosis (TB) caused by *Mycobacterium tuberculosis* (*Mtb*) continues to be one of the leading causes of death and morbidity globally, claiming 1.2 million lives in 2018.[1] The emergence and spread of multi drug-resistant (MDR) and extensively drug-resistant (XDR) strains of *Mtb* that are resistant to the first- and second-line drugs have further exacerbated the situation.[2] The rise in anti-microbial resistance warrants the search for new drugs with unique modes of action that can bypass existing modes of resistance or can be used as adjunctive therapy to compensate for those that are vulnerable to promoting resistance. While considerable progress has been made toward establishing a TB drug pipeline, the high attrition rate in clinical development reinforces the need to continually replenish the pipeline with high-quality leads that act through the inhibition of novel targets.[3]

In light of the above, we have been engaged in early TB drug discovery to identify and progress new chemical series with potentially novel modes of action lacking cross-resistance with existing drugs.[4,5] One approach to identify compounds with a novel mode of action is to phenotypically screen compound libraries against *Mtb* growing under different media conditions with different carbon sources followed by a biology triage process to weed out actives hitting frequently encountered targets such as the respiratory system (e.g., QcrB) and cell–wall synthesis (e.g., MmpL3 and DprE1), as well as DNA damaging agents. Herein, we describe structure–activity relationship (SAR) and target identification studies of one novel chemical series, 2-pyrazolylpyrimidinones—represented in Figure 1. This series was identified through high-throughput screening of a Medicines for Malaria Venture (MMV) compound library.

Received: October 1, 2020
Published: January 4, 2021

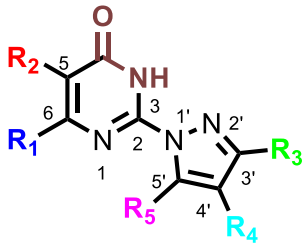

Figure 1. Generic structure of pyrazolylpyrimidones.

RESULTS AND DISCUSSION

Phenotypic Hits with a Novel Mode of Action. A high-throughput screen of a ~530,000 diverse set of compounds from MMV compound library against *Mtb* was conducted at the National Institute of Allergy and Infectious Diseases of the National Institutes of Health (NIAID/NIH, U.S.). Reconfirmed hits were followed up for determination of minimum inhibitory concentration (MIC) on multiple media that identified a cluster of pan-active pyrazolylpyrimidinones represented by compounds **1** and **2** (Table 1). The biology triage of these actives

Table 1. Properties of the Hits from the MMV Library Screen[a]

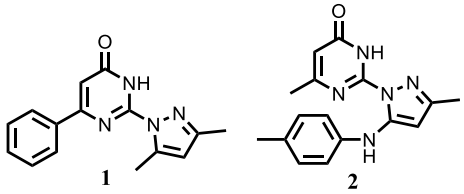

Properties	1	2
MIC 7H9/ADC/Tw (μM)	0.6	2
MIC GAST-Fe (μM)	0.02	0.02
MIC 7H9/Glu/BSA/Tx (μM)	1.5	2
MIC 7H9/Glu/Cas/Tx (μM)	0.3	0.4
MIC 7H9/DPCC/Cas/Tx (μM)	0.4	0.2
MIC 7H9/DPCC/Chol/BSA/Tx (μM)	1.5	6
Vero IC_{50} (μM)	8	1.2
HepG2 IC_{50} (Glu/Gal μM)	4/4	ND
$Solubility_{pH7.4}$ (μM)	10	<5
$LogD_{pH7.4}$	2.5	2.2
Molecular Weight	266.304	295.346
Microsomal stability H/R/Mo %remaining	98/69/22	73/76/78

[a]MIC—minimum inhibitory concentration against *Mtb* H37Rv; 7H9—Middlebrook 7H9; ADC—albumin−dextrose−catalase supplement; Tw—Tween 80; GAST-Fe—glycerol-alanine-salts with Tween and iron salts; Glu—glucose; BSA—bovine serum albumin; Tx—Tyloxapol; Cas—Casitone; DPCC—dipalmitoylphosphatidylcholine and cholesterol; Chol—cholesterol; H/R/Mo—human/rat/mouse; IC_{50}—50% inhibitory concentrations; $solubility_{pH7.4}$—aqueous solubility at pH 7.4.

(described in the target identification section), suggestive of a unique mechanism of action (MoA), generated further interest in the exploration of these hits. We recognized that pyrazolylpyrimidinones potentially possess iron-chelating properties by virtue of their two sp2 heteroatoms in a 1,4-relationship on adjacent rings, which might play a crucial role in the SAR and mode of action.[6] During these studies, we came across the related pyrazolopyrimidinone (PZP, Figure 2a) compound reported as an intracellular iron chelator in *Mtb*.[7] PZP is

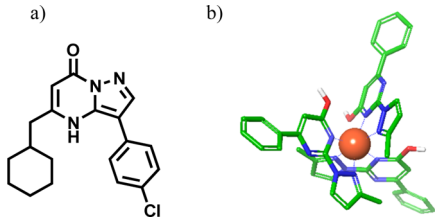

Figure 2. (a) Structure of PZP; and (b) depiction of metal chelation by pyrazolylpyrimidinone **1**.

reported to chelate iron through the pyrimidinone carbonyl and 2-position pyrazole nitrogen. Similarly, bidentate iron chelation by the pyrazolylpyrimidinones from the pyrimidinone nitrogen and pyrazole nitrogen as depicted in Figure 2b may be hypothesized. A single-crystal X-ray structure of the pyrazolylpyridines−Fe complex is reported in the literature which supports this hypothesis.[8,9] This aspect of metal chelation by the compounds was considered while planning further SAR exploration and target identification studies with the series.

Synthesis. In order to explore the SAR profiles of the series, various routes were explored toward the synthesis of diverse range of analogues as represented by compounds **3**−**54** in Tables 2−5. To facilitate exploration of a broad array of substituents off the pyrazole ring and pyrimidinone core, a concise and scalable synthesis leading to an advanced intermediate was desired. As summarized in Scheme 1, this was achieved by the ring formation reaction of 6-substituted-2-thiomethyl-pyrimidin-4-one **55** via condensation of the appropriate β-keto-ester and thiourea, and subsequent methylation of the thiol.[10] Intermediates **55a**−**g** were reacted with hydrazine hydrate in refluxing ethanol to give the versatile 2-hydrazinylpyrimidin-4(1*H*)-ones **56a**−**g**, which gave access to analogues for SAR exploration on the pyrazole ring and the R1 substituent on the pyrimidinone core. Similarly, substitution of a phenyl group at the R2 position was achieved through bromination at C5 of 6-methyl-2-thiomethyl-pyrimidin-4-one (**55**, R1 = CH_3) followed by a Suzuki cross-coupling reaction with phenyl boronic acid to provide **55h**, which was then treated with hydrazine to form **56h**.

The Knorr reaction was used to incorporate the 3,5-dimethylpyrazole via an acid-catalyzed condensation of hydrazine precursors **56a**−**h** and acetylacetone. This led to hit compound **1** and related analogues exploring the R1 (**11**, **12**, **19**, **20**, and **21**) and R2 (**8**−**9**) positions of the pyrimidinone core as well as quinazolin-4(3*H*)-one analogue (**10**). In addition, 2-hydrazinylpyrimidin-4(1*H*)-one **56a** and **56d** were reacted with (*Z*)-3-aminocrotonitrile to afford 5-aminopyrazolylpyrimidinone analogues **14** and **33**,[11] which allowed for several transformations to be carried out to expand SAR exploration on the pyrazole ring later described in Scheme 7. To explore polar modifications off the pyrazole ring, a mixture of 2-(5-amino-3-methyl-1*H*-pyrazol-1-yl)-6-phenylpyrimidin-4(3*H*)-one **14** and pyridine in dichloromethane was treated with acetyl chloride to provide *N*-acetyl amide **15**.[2] In addition, hydrazine **56a** was heated with ethyl acetoacetate in acidic ethanol to yield pyrazolone **13**.

Syntheses of compounds **3**−**7** (Table 2) with changes in the central core ring are summarized in Scheme 2. Compounds masking the pyrimidinone amide were synthesized from compound **1** via a Mitsunobu reaction to form methyl ether **3** and N-methylation of **1** with iodomethane using potassium carbonate in *N*,*N*-dimethylformamide (DMF) to afford *N*-

https://dx.doi.org/10.1021/acs.jmedchem.0c01727
J. Med. Chem. 2021, 64, 719−740

Table 2. Pharmacophore Evaluation of Pyrazolylpyrimidinones[a]

Compound	Structure	MIC (μM)	Solubility (μM)	Cytotoxicity (CHO IC_{50} μM)	SI
1	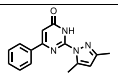	1.5	10	8	5
3	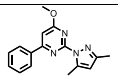	>50	200	>50	
4	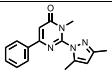	>50	200	357 (V)	
5	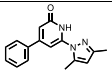	>50	185	>50	
6	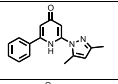	>50	120	>50	
7	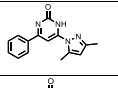	2	30	10	5
8	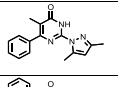	2	120	25	12.5
9	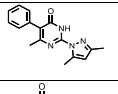	9	190	9	1
10	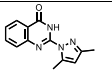	3	150	6	2
11	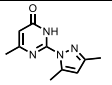	30	180	325 (V)	10.8
12	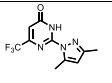	12	200	150	12.5
13	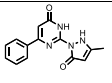	>125	190	ND	
14	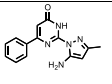	3	180	9 (V)	3
15	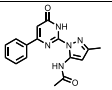	6	150	35 (V)	5.8
16	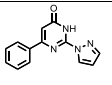	50	190	>50	>1
17	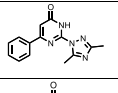	>125	130	>50	
18	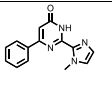	20	200	4	0.2

[a]MIC were measured in Middlebrook 7H9/Glu/BSA/Tyloxapol media at day 7; IC_{50}—50% inhibitory concentrations; solubility—aqueous solubility measured at pH 7.4; CHO—an epithelial cell-line derived from the ovary of the Chinese hamster; and V—Vero cell-line; SI—selectivity index between CHO IC_{50} and *Mtb* MIC.

methyl pyrimidinone **4**. The nucleophilic aromatic substitution reaction of 2,6-dichloro-4-iodopyridine with sodium methoxide gave intermediates **57** and **58** in a 2:1 ratio, which upon separation allowed for the synthesis of compounds **5** and **6**,

Table 3. Polar Substitutions on Pyrimidinone[a]

Compound	Structure	MIC (μM)	Solubility (μM)	Cytotoxicity (CHO IC_{50} μM)	SI
19	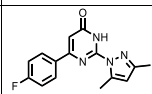	1.2	35	4	3.3
20	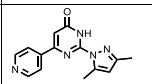	9	180	>50	>5.5
21	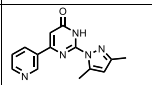	50	200	>50	>1
22	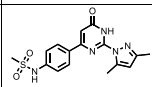	>125	20	>50	
23	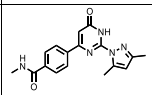	>50	70	>50	
24	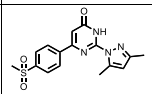	>50	8	>50	
25	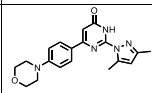	>125	40	ND	
26	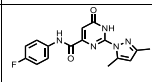	25	200	>50	≥2
27	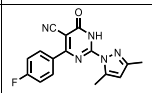	>50	30	>50	
28	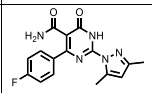	>50	110	ND	
29	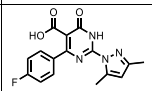	>50	190	>50	

[a]MIC—were measured in Middlebrook 7H9/Glu/BSA/Tyloxapol media at day 7; IC_{50}—50% inhibitory concentrations; solubility—aqueous solubility measured at pH 7.4; CHO—an epithelial cell-line derived from the ovary of the Chinese hamster; and SI—selectivity index between CHO IC_{50} and *Mtb* MIC.

respectively. Briefly, the three-step synthesis from **57** and **58** involved a Suzuki cross-coupling reaction with phenylboronic acid to afford intermediates **59** and **60**, respectively, followed by a Buchwald Hartwig amination to introduce the pyrazole (intermediates **61** and **62**, respectively), and finally O-demethylation with boron tribromide to afford compounds **5** and **6**, respectively.

Pyrimidin-2(1*H*)-one **7** was synthesized by the cyclization of ethyl benzoylacetate with urea to provide uracil **63**, which was then reacted with phosphorus oxychloride in the presence of a catalytic amount of DMF to give 2,4-dichloropyrimidine **64** (Scheme 2).[12] The activated 2,4-dichloropyrimidine readily undergoes nucleophilic substitution with the pyrazole at the 4-chloro position by heating in the microwave at 80 °C (intermediate **65**) and subsequent hydrolysis of 2-Cl afforded

https://dx.doi.org/10.1021/acs.jmedchem.0c01727
J. Med. Chem. 2021, 64, 719−740

Table 4. SAR at the Pyrazole R5 Position[a]

Compound	Structure	MIC (μM)	Solubility (μM)	Cytotoxicity (CHO IC_{50} μM)	SI
30	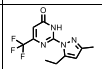	12	200	108	9
31	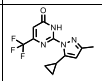	12	160	78	6.5
32	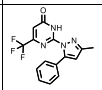	25	200	>50	>2
33	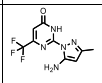	20	200	120	6
34	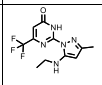	6.25	85	8	1.28
35	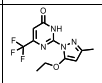	25	120	>50	>2
36		58	200	ND	
37	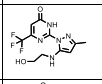	37	200	ND	
38		2	200	17	8.5
39	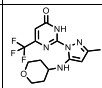	1.56	50	18	11.5
40	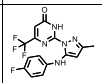	1.56	15	20	12.8
41	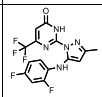	0.3	<5	8	26
42	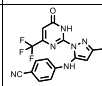	9.4	75	20	2.1
43	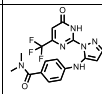	>50	200	ND	
44	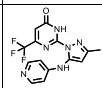	>50	20	ND	
45	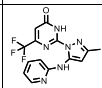	0.9	25	23	25
46	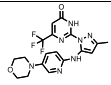	2.3	180	1.3	0.6
47	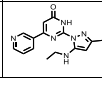	6.25	90	>50	>8

[a]MIC—were measured in Middlebrook 7H9/Glu/BSA/Tyloxapol media at day 7; IC_{50}—50% inhibitory concentrations; solubility—aqueous solubility measured at pH 7.4; CHO—an epithelial cell-line derived from the ovary of the Chinese hamster; and SI—selectivity index between CHO IC_{50} and *Mtb* MIC.

Table 5. SAR at the Pyrazole R3 Position[a]

Compound	Structure	MIC (μM)	Solubility (μM)	Cytotoxicity (CHO IC_{50} μM)	SI
48	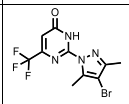	25	200	>50	>2
49	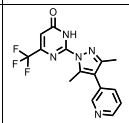	>50	195	ND	
50	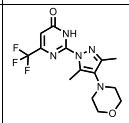	6.25	160	>50	>8
51	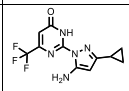	25	10	24	1
52	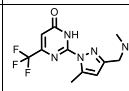	>50	200	ND	
53	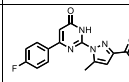	>50	155	ND	
54	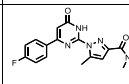	>50	65	ND	

[a]MIC—were measured in Middlebrook 7H9/Glu/BSA/Tyloxapol media at day 7; IC_{50}—50% inhibitory concentrations; solubility—aqueous solubility at pH 7.4; CHO—an epithelial cell-line derived from the ovary of the Chinese hamster; and SI—selectivity index between CHO IC_{50} and *Mtb* MIC.

compound **7**, with the carbonyl functionality between the ring nitrogens.

Compounds **16** and **17** (Table 2), in which the pyrazole ring was replaced with other 5-membered heterocycles, were synthesized in a similar manner from 2,4-dichloro-6-phenylpyrimidine **64** (Scheme 3). The alkaline hydrolysis of intermediate **64** with 20% aqueous sodium hydroxide occurred primarily at the 4-Cl position to provide advanced intermediate **66** (isomer ratio 70:30),[13] which was reacted with the corresponding 5-membered heterocycle to displace 2-Cl using cesium carbonate under microwave heating at 80 °C (Scheme 3). Compound **18** with an *N*-methylimidazole was synthesized by condensing 1-methyl-1*H*-imidazole-2-carboximidamide with ethyl benzoylacetate in low yields.

In order to introduce groups with polar functionalities at the R1 and R2 positions on the pyrimidinone core, 2,4,6-trichloropyrimidine was a useful and accessible starting material when the appropriate *β*-keto-ester was not readily available to pursue synthetic routes, as shown in Schemes 1 and 3. Treatment of 2,4,6-trichloropyrimidine in aqueous 1,4-dioxane, brought to the alkaline reaction with NaOH, led to hydrolysis at room temperature with the formation of 4,6-dichloro-2-hydroxypyrimidine **67** and 2,6-dichloropyrimidin-4(3*H*)-one **68**, with the former precipitating out as the sodium salt (Scheme 4).[14] The filtrate was concentrated to approximately half the volume and cooled to afford a precipitate which was filtered off and acidified to pH 2 using 5 N HCl to give the required

https://dx.doi.org/10.1021/acs.jmedchem.0c01727
J. Med. Chem. 2021, 64, 719−740

Scheme 1. Synthetic Route to Explore R1 and R2 on the Pyrimidinone and Polar Modifications at R5 on the Pyrazole[a]

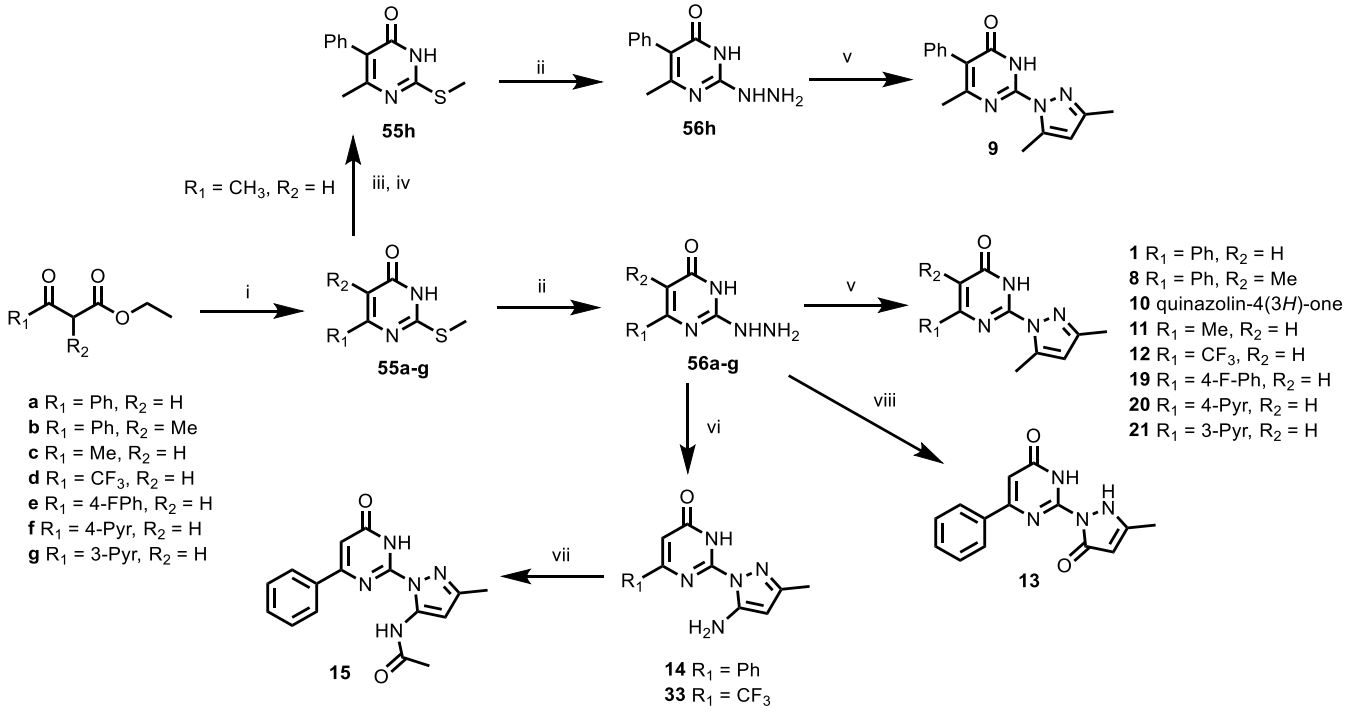

[a]Reagents and conditions: (i) (a) thiourea, KOH, EtOH, reflux (b) iodomethane, NaOH, H_2O/EtOH; (ii) $NH_2NH_2{\cdot}H_2O$, EtOH, reflux; (iii) Br_2, AcOH, 60 °C; (iv) phenylboronic acid, $Pd(PPh_3)_2Cl_2$, 1,4-dioxane, K_2CO_3; (v) acetylacetone, EtOH, AcOH, reflux; (vi) 3-aminocrotonitrile, EtOH, reflux; (vii) acetyl chloride, pyridine, CH_2Cl_2; and (viii) ethyl acetoacetate, EtOH, AcOH, reflux.

Scheme 2. Synthetic Routes to Access Core Modifications[a]

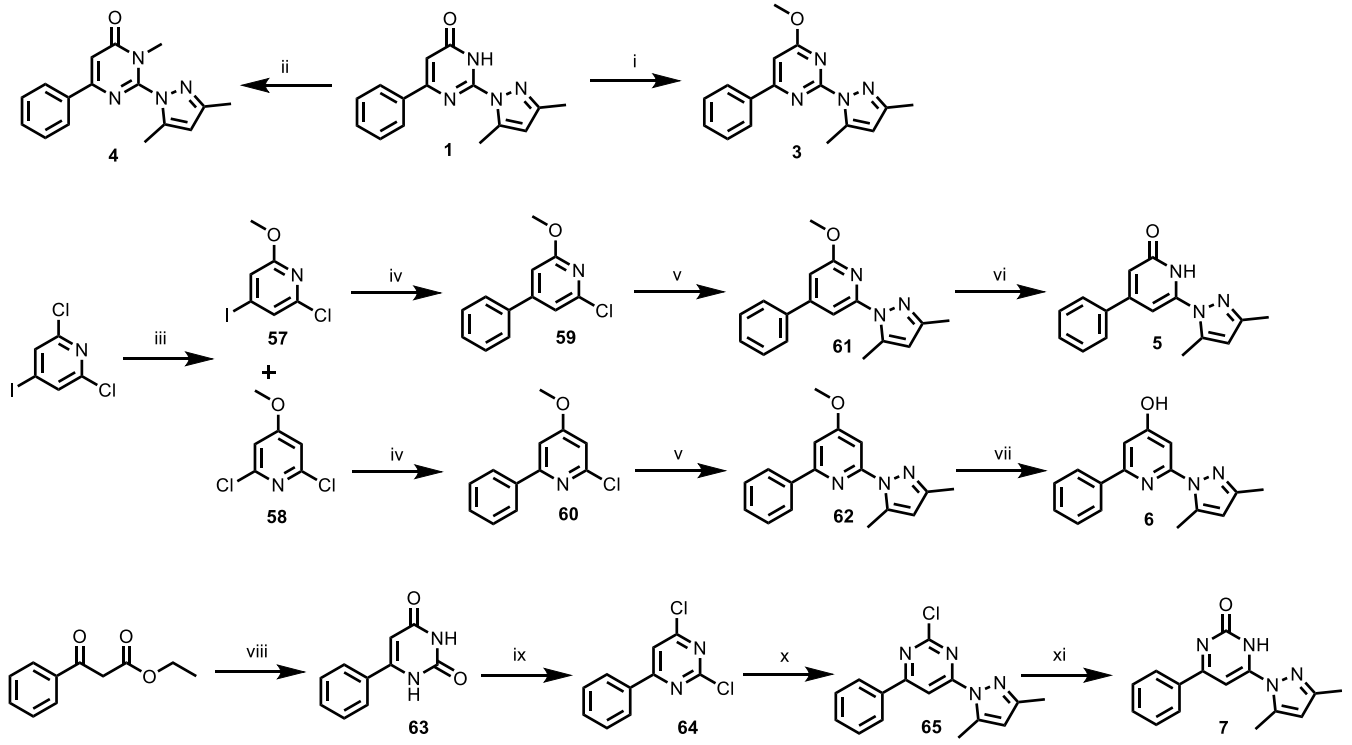

[a]Reagents and conditions: (i) MeOH, PPh_3, DIAD, THF, 25 °C; (ii) MeI, K_2CO_3, DMF, 100 °C; (iii) $NaOCH_3$, MeOH, 80 °C; (iv) phenylboronic acid, $Pd(PPh_3)_2Cl_2$, K_2CO_3, 1,4-dioxane, reflux; (v) 3,5-dimethylpyrazole, xanphos, $Pd(OAc)_2$, Cs_2CO_3, 1,4-dioxane, 130 °C; (vi) BBr_3, MeOH; (vii) BBr_3, CH_2Cl_2; (viii) urea, 1,4-dioxane, 140 °C, microwave; (ix) $POCl_3$, DMF; (x) 3,5-dimethylpyrazole, Cs_2CO_3, 1,4-dioxane, 80 °C, microwave; and (xi) 20% aq NaOH, 80 °C.

https://dx.doi.org/10.1021/acs.jmedchem.0c01727
J. Med. Chem. 2021, 64, 719−740

Scheme 3. Synthetic Route for Pyrazole Replacements[a]

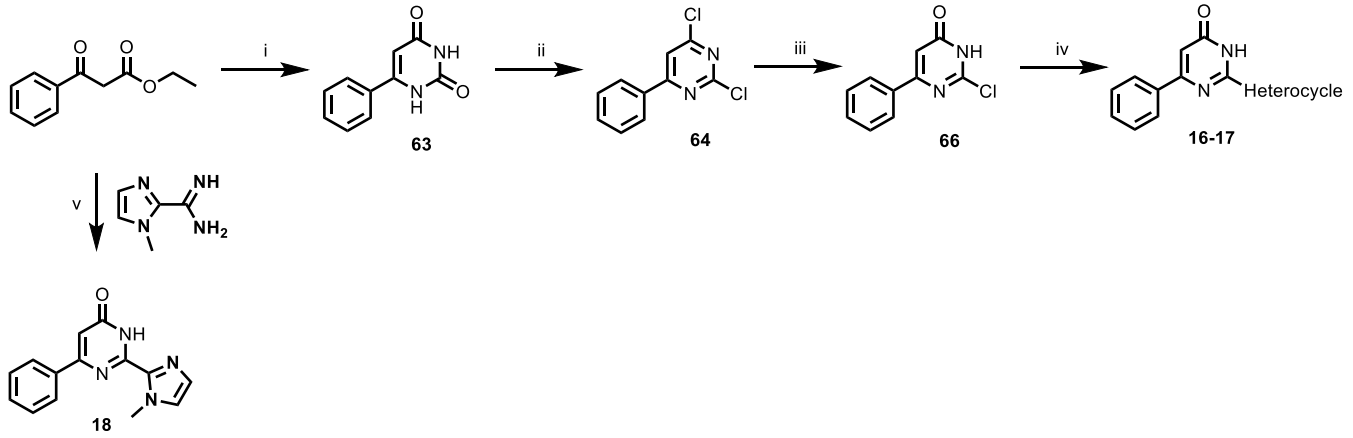

[a]Reagents and conditions: (i) urea, 1,4-dioxane, 140 °C, microwave; (ii) $POCl_3$, DMF; (iii) 20% aq NaOH, 80 °C (iv) 5-membered heterocycle, Cs_2CO_3, 1,4-dioxane, 80 °C, microwave; and (v) EtOH, reflux, 1 h.

Scheme 4. Synthetic Route to Polar Substitutions on R1 of the Pyrimidinone[a]

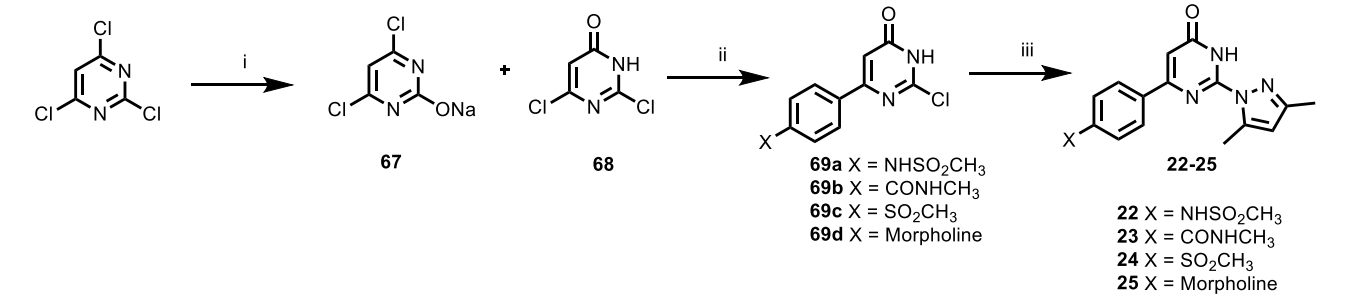

[a]Reagents and conditions: (i) aqueous NaOH, dioxane; (ii) boronic acid, Cs_2CO_3, $Pd(OAc)_2$, dppf, 1,4-dioxane, 70 °C or K_2CO_3, $PdCl_2(dppf)_2$, 1,4-dioxane, 70 °C; and (iii) 3,5-dimethylpyrazole, Cs_2CO_3, 1,4-dioxane, 130 °C, microwave.

Scheme 5. Synthetic Route to Amide 26[a]

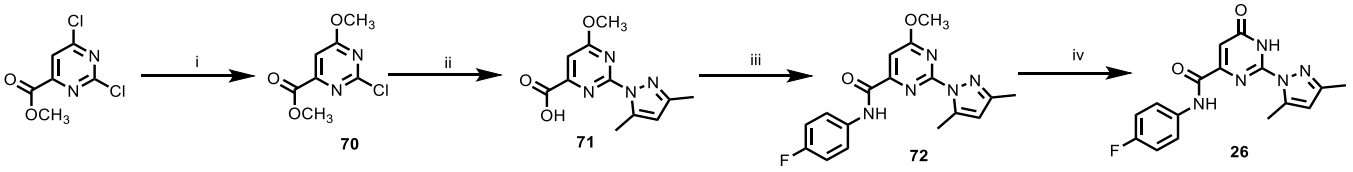

[a]Reagents and conditions: (i) CH_3ONa, THF, 0 °C; (ii) 3,5-dimethylpyrazole, Cs_2CO_3, 1,4-dioxane, 110 °C, microwave; (iii) 4-fluoroaniline, HATU, Et_3N, DMF; and (iv) BBr_3, CH_2Cl_2.

regioisomer **68**, in approximately 40% yield. The reactivity of each position of the pyrimidine halides follows the general order C6(4) > C2 ≫ C5.[15] A strong preference for the C6 position has been observed in Suzuki cross-coupling reactions.[16−20] Coupled with the use of a lower temperature for the Suzuki coupling, this allowed for the sequential introduction of different substituents.

Thus, 2,6-dichloropyrimidin-4(3*H*)-one **68** underwent a Suzuki cross-coupling with the appropriate boronic acid, using $Pd(OAc)_2$/dppf or $PdCl_2(dppf)_2$ as the catalyst to afford compounds **69a−d**. Coupling of intermediates **69a−d** with 3,5-dimethylpyrazole was achieved by heating to 130 °C under microwave irradiation using 15 mol % $Pd_2(dba)_3$, xanphos, and Cs_2CO_3 in 1,4-dioxane to afford the desired compounds **22−25** (Table 3). A slightly modified procedure, as shown in Scheme 5, was used to prepare amide **26**. Methyl 2,6-dichloropyrimidine-4-carboxylate was treated with sodium methoxide at 0 °C to obtain intermediate **70**. Intermediate **70** was then reacted with 3,5-dimethylpyrazole under microwave heating using Cs_2CO_3 as a base to give acid **71**, which was followed by subsequent in situ hydrolysis of the methyl ester. Acid **71** was coupled with 4-fluoroaniline using 1-[bis(dimethylamino)methylene]-1*H*-1,2,3-triazolo[4,5-*b*]pyridinium 3-oxid hexafluorophosphate (HATU) to give amide intermediate **72**, which was demethylated using boron tribromide in dichloromethane to give compound **26**.

To determine if polarity at the R2 position on the pyrimidinone core was tolerated, compounds **27−29** (Table 3) were synthesized using the route, as shown in Scheme 6. 4-Fluorobenzaldehyde was condensed with thiourea and ethyl cyanoacetate using potassium hydroxide in refluxing ethanol to give 2-mecapto-5-cyanopyrimidinone intermediate **73**.[21] The thiol of intermediate **73** was methylated using methyl iodide in the presence of sodium hydroxide followed by displacement with hydrazine in refluxing ethanol to give 2-hydrazinyl-5-

https://dx.doi.org/10.1021/acs.jmedchem.0c01727
J. Med. Chem. 2021, 64, 719−740

Scheme 6. Synthetic Route to Polar Substitutions on R2 of the Pyrimidinone[a]

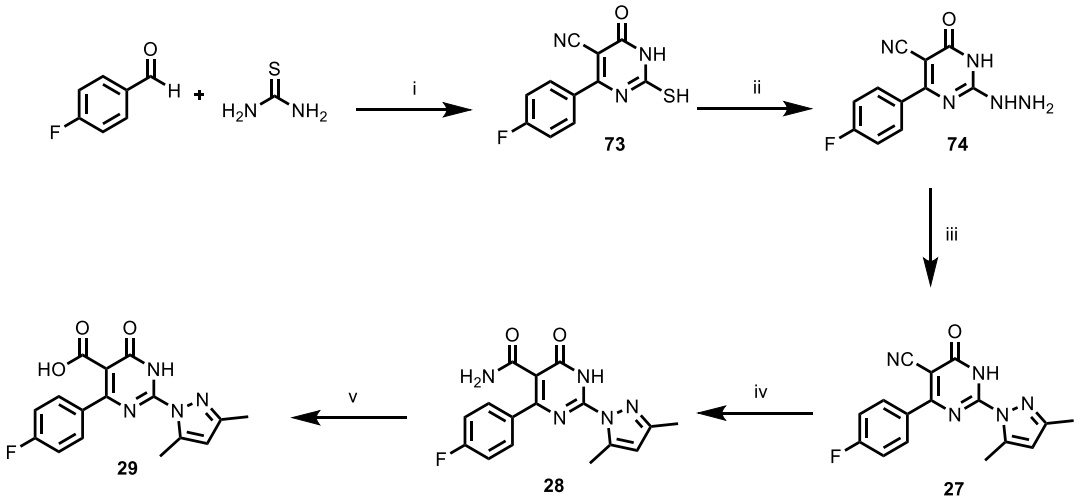

[a]Reagents and conditions: (i) ethyl 2-cyanoacetate, KOH, ethanol, reflux; (ii) (a) MeI, NaOH, H_2O (b) $NH_2NH_2{\cdot}H_2O$, EtOH, reflux; (iii) acetylacetone, AcOH, EtOH, 85 °C; (iv) H_2SO_4, 80 °C; and (v) *tert*-butyl nitrite, AcOH, 75 °C.

Scheme 7. Synthetic Routes Used to Explore the Pyrazole R5 Position[a]

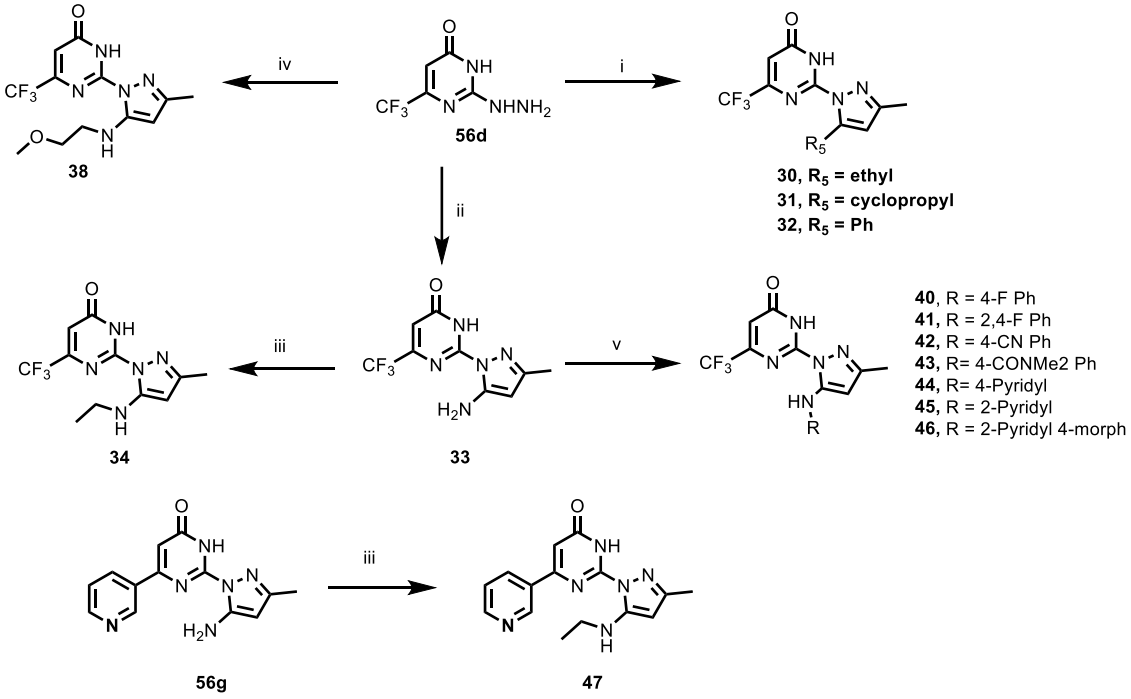

[a]Reagents and conditions: (i) diketone, EtOH, AcOH, reflux; (ii) 3-aminocrotonitrile, EtOH, reflux; (iii) acetaldehyde, DMF, AcOH, $NaCNBH_4$, MeOH, 25 °C; (iv) *N*-(2-methoxyethyl)-3-oxobutanamide, Lawesson's reagent, THF, 25 °C; and (v) Cs_2CO_3, $Pd_2(dba)_3$, XantPhos, 1,4-dioxane, aryl halide, 120 °C

cyanopyrimidinone intermediate **74**. This intermediate was then condensed with acetylacetone by heating in acetic acid-ethanol at 85 °C to obtain compound **27**, which was hydrolyzed to amide **28** by heating in concentrated sulfuric acid at 85 °C.[22] The conversion of amide **28** to acid **29** was achieved via nitrosation by heating with *tert*-butyl nitrite in acetic acid at 85 °C followed by hydrolysis.[23]

Compounds **30**–**47** (Table 4) were synthesized to explore the SAR around the R5 position of the pyrazole ring, keeping the C6-position on the pyrimidinone core fixed as trifluoromethyl. Using the same methodology, as shown Scheme 1, the condensation of **56d** with the corresponding 1,3-dicarbonyl compound afforded compounds **30**–**32** exclusively as one regioisomer as confirmed by NOESY NMR (Scheme 7). In addition, **56d** provided access to compound **33**, which served as a versatile intermediate and allowed for several transformations to form N-substituted pyrazole derivatives. The reductive amination of acetaldehyde with **33** in the presence of sodium cyanoborohydride in methanol gave ethylaminopyrazole **34**. Attempts to synthesize the *N*,*N*-dialkyl derivative from compound **34** failed as the corresponding derivatives decomposed on standing. Compound **47** was synthesized in the same

https://dx.doi.org/10.1021/acs.jmedchem.0c01727
J. Med. Chem. 2021, 64, 719−740

Scheme 8. Synthetic Route to Compounds 36−39[a]

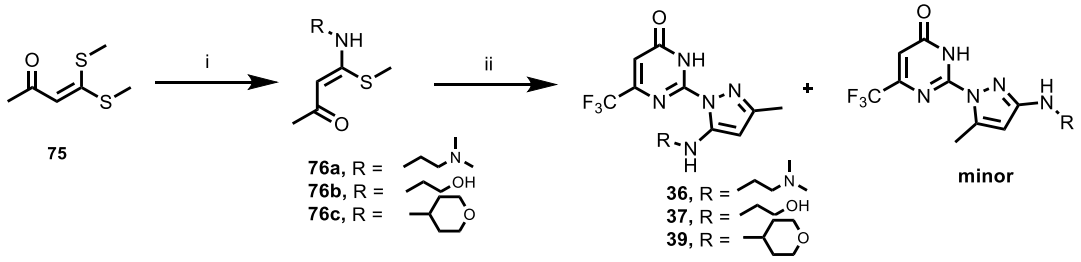

[a]Reagents and conditions: (i) NH_2-R, EtOH, reflux; (ii) **33**, AcOH, EtOH, 100 °C.

Scheme 9. Synthesis of Compound 35[a]

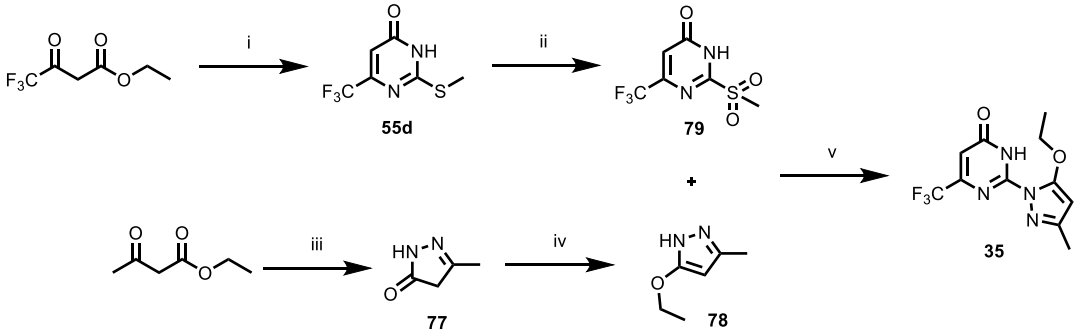

[a]Reagents and conditions: (i) (a) thiourea, KOH, EtOH and (b) MeI, NaOH, H_2O; (ii) *m*CPBA, CH_2Cl_2, 25 °C; (iii) N_2H_2. H_2O, EtOH; (iv) EtI, K_2CO_3, DMF, 70 °C; and (v) Cs_2CO_3, 1,4-Dioxane, 130 °C.

Scheme 10. Synthesis of Compounds with Pyrazole C4 Substitutions[a]

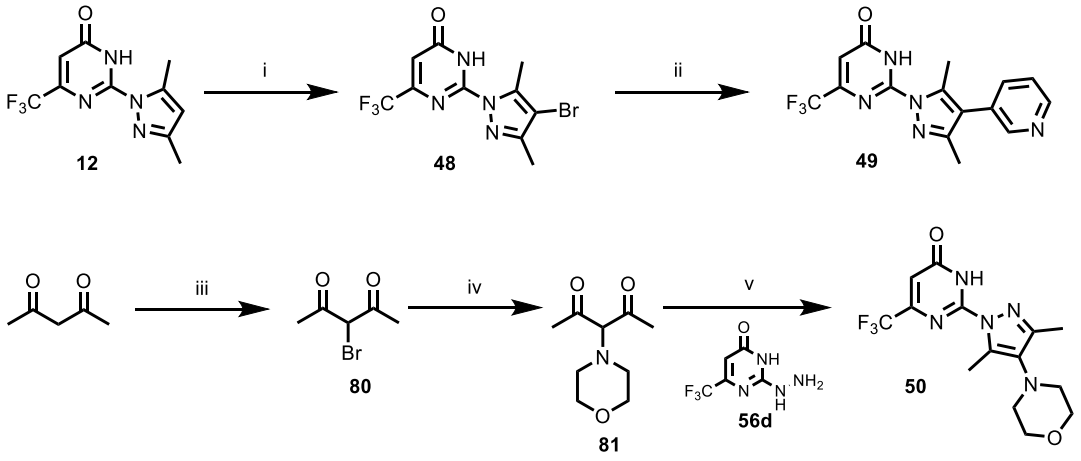

[a]Reagents and conditions: (i) Br_2, AcOH, 100 °C, 2h; (ii) pyridine-3-boronic acid, K_2CO_3, Pd(dppf)Cl_2, THF/water (10:1), 70 °C, 16h; (iii) *N*-bromosuccinamide, *p*-toluene sulphonic acid, CH_2Cl_2; 0 °C; (iv) morpholine, Et_3N, CH_2Cl_2; and (v) EtOH/AcOH reflux, 16 h.

manner by reductive amination of acetaldehyde with 2-hydrazineyl-6-(3-pyridinyl)pyrimidinone **56g**. The synthesis of 5-(aryl-amino)pyrazoles **40−46** was achieved via a Buchwald Hartwig amination of **33** and the corresponding aryl halide.

Compound **38** was synthesized from hydrazine **56d** and *N*-(2-methoxyethyl)-3-oxobutanamide with Lawesson's reagent, which allows for the efficient installation of substituted-5-amino groups on the pyrazole core in a single step.[24] However, this methodology failed in the case of the synthesis of compounds **36**, **37**, and **39**, with 2-(5-hydroxy-3-methyl-1*H*-pyrazol-1-yl)-6-(trifluoromethyl)pyrimidin-4(3*H*)-one being obtained as the major product. An alternate highly regioselective route to 5-(substituted-amino)pyrazoles **36**, **37**, and **39** was achieved following a modified literature procedure.[25]

As shown in Scheme 8, the displacement of one methylthio group of the *α*-oxoketene dithioacetal **75**[26,27] by the appropriate amine in the presence of acetic acid in ethanol afforded the *N*,*S*-acetals **76a-c**, which were useful three-carbon 1,3-electrophiles.[28] Cyclocondensation with hydrazine **56d** in refluxing ethanol, gave access to 5-(substituted-amino)pyrazoles **36**, **37**, and **39**. The regioisomeric products with 3-(substituted-amino)pyrazoles could be isolated in minor quantities and showed much less potent activity against *Mtb* (data not shown).

Compound **35**, with an *O*-ethyl group at R5, was synthesized, as shown in Scheme 9. The condensation of ethyl acetoacetate

https://dx.doi.org/10.1021/acs.jmedchem.0c01727
J. Med. Chem. 2021, 64, 719−740

Scheme 11. Synthesis of Compounds with Pyrazole C3 Modifications[a]

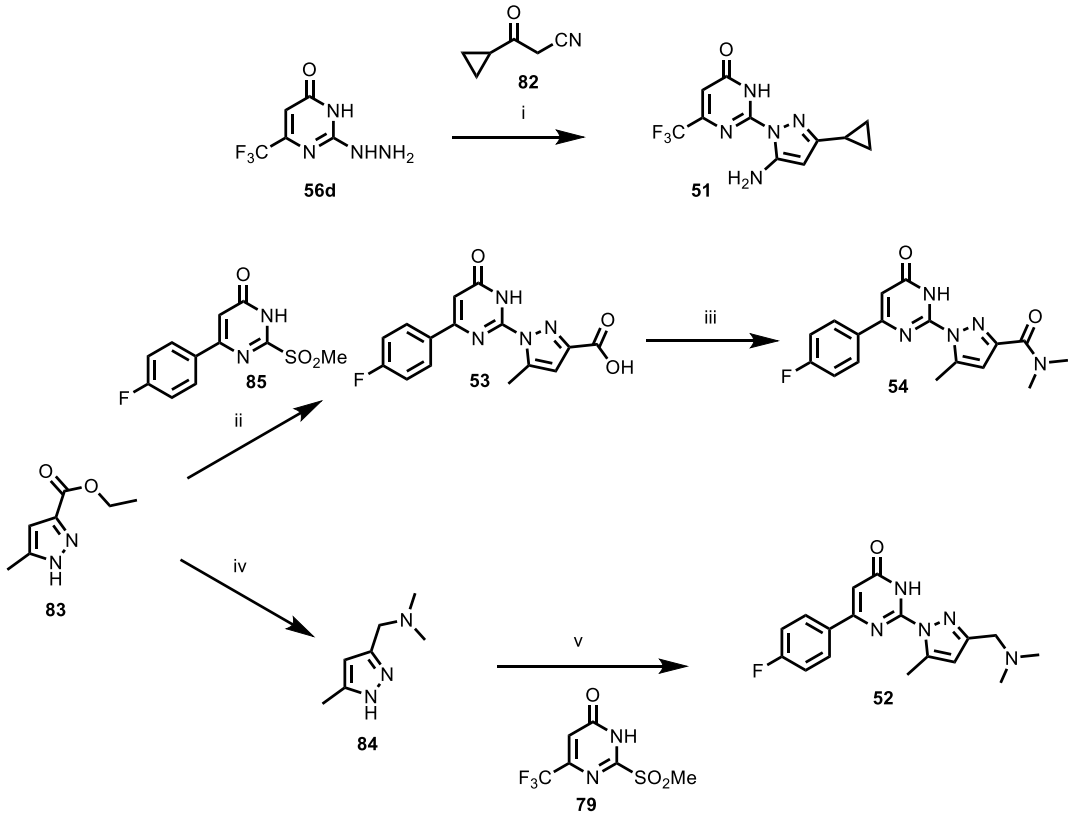

[a]Reagents and conditions. (i) DMF, 130 °C, 2 h; (ii) Cs_2CO_3, 1,4-dioxane, 130 °C, microwave; (iii) *N*,*N*-dimethylamine, HATU, Et_3N, DMF; (iv) (a) DIBALH, CH_2Cl_2, −78 °C; (b) *N*,*N*-dimethylamine, $NaCNBH_3$, THF, RT, 24 h; and (v) Cs_2CO_3, 1,4-dioxane, 130 °C, microwave.

and hydrazine delivered pyrazolone **77**, which on subsequent *O*-ethylation with ethyl iodide gave **78**. Intermediate **78** was coupled with **79**, synthesized by the oxidation of thiomethylpyrimidin-4-one **55d** with *m*CPBA to yield **35**.

Compounds **48**−**50** with substitutions on the pyrazole C4 position were synthesized, as shown in Scheme 10. The bromination of compound **12** gave compound **48**, which on Suzuki cross-coupling with pyridine-3-boronic acid gave compound **49**. Attempts to displace C4-Br of **48** with morpholine to synthesize compound **50** were unsuccessful. In an alternative route, the morpholine ring was preinstalled on acetylacetone via bromination with *N*-bromosuccinimide (intermediate **80**) followed by the reaction with morpholine in the presence of triethylamine to give intermediate **81**. This intermediate was then condensed with hydrazine **56d** by refluxing in ethanol-acetic acid to give compound **50**.

Compound **51** was synthesized in a similar fashion to compound **33**, by condensing hydrazine **56d** with 3-cyclopropyl-3-oxopropanenitrile (**82**) (Scheme 11). The synthesis of compounds **52**−**54** was accomplished from **83**, as shown in Scheme 11. The reaction of **83** with **85** under microwave heating gave acid **53**. This compound was then coupled with dimethylamine using HATU to give compound **54**. Pyrazole ester **83** was converted to the corresponding dimethylaminomethyl derivative **84** via a standard two-step protocol involving the reduction of the ester to the aldehyde followed by reductive amination with dimethylamine. Intermediate **84** was reacted with 2-methylsulphonylpyrimidinone **79** under microwave heating to obtain compound **52**.

Formal Hit Assessment to Determine the Pharmacophore Critical for Antitubercular Activity. Although the initial hits, **1** and **2** (Table 1), showed reasonably potent antitubercular activity (MIC < 2 μM), they suffered from unfavorable physicochemical properties including low solubility, low to moderate microsomal metabolic stability (MS), and a low selectivity index (SI) between *Mtb* MIC and mammalian cell toxicity as determined by measuring 50% inhibitory concentrations (IC_{50}) determined against a CHO cell-line (an epithelial cell-line derived from the Chinese-hamster ovary). A formal hit assessment study was undertaken to determine the minimum pharmacophoric features critical for antitubercular potency and to understand the SAR features needed to improve the SI. Initially, compounds with single point modifications on the pyrimidinone and pyrazole portions of the molecule were synthesized and profiled in a first wave of assays comprising *Mtb* MIC, CHO IC_{50}, and aqueous solubility. The substituents on the pyrimidinone and pyrazole rings were labeled R1-R5, as shown Figure 1 (see Table 2). Masking of the pyrimidinone amide as $-OCH_3$ (**3**) or *N*-CH_3 (**4**) abolished the *Mtb* activity, indicating the essentiality of the NH, which might be involved in the critical hydrogen bond (HB) donor−acceptor interactions with the target. Each of the nitrogens of the pyrimidinone ring were found to be essential for maintaining *Mtb* activity (**5** and **6**). Interestingly, compound **7** with the carbonyl functionality between the ring nitrogens pyrimidin-2(1*H*)-one vs pyrimidin-4(3*H*)-one as in **1** maintained similar *Mtb* activity. The additional SAR explorations in this work were limited to the pyrimidin-4(3*H*)-one core as in compound **1**, considering the ease of synthesis.

https://dx.doi.org/10.1021/acs.jmedchem.0c01727
J. Med. Chem. 2021, 64, 719−740

Compound **8** with a methyl group added at the pyrimidinone C5 (R2) position, while keeping a phenyl substituent at C6 (R1), retained a good MIC value (2 μM) while improving aqueous solubility (120 μM) and the SI (12.5) for cytotoxicity. However, isomeric compound **9** with C5-phenyl (R2) and C6-methyl (R1) showed a poor MIC value (9 μM) with a lower SI of 1, whereas the fusion of the phenyl ring with the pyrimidinone ring to form the corresponding quinazolinone (compound **10**) retained potency but with a low SI of only 2. A phenyl substituent at the R1 (pyrimidinone C6) position was necessary to maintain *Mtb* activity. Compounds **11** and **12** with CH_3 and CF_3 groups, respectively, at R1 instead of the phenyl substituent showed a 10−15-fold loss in activity. As compound **12** with the CF_3 group at R1 showed higher solubility and SI relative to **1**, this modification was included in further explorations for potency and selectivity. Overall, these SAR observations suggested the requirement for hydrophobic substitutions on the pyrimidinone ring for the retention of potent *in vitro* activity against *Mtb*.

A few polar modifications on the pyrazole ring were attempted in order to evaluate the scope of reducing lipophilicity and improving drug-like properties. Changing the C5′-methyl (R5) on the pyrazole to oxygen abolished the activity as observed for compound **13**, whereas an amino group at the C5′-position as in compound **14** resulted in the retention of activity comparable to compound **1** (3 μM) and significantly improved solubility (180 μM). Unfortunately, this polar modification did not improve the SI. *N*-acetyl amide derivative **15** retained the activity and SI profile similar to parent amine **14**. Compound **16**, with an unsubstituted pyrazole, lost potency considerably (MIC 50 μM). A similar loss in potency was observed when the pyrazole ring was replaced with other 5-membered rings like triazole or imidazole, as in compounds **17** and **18**, respectively. This suggests the critical nature of an appropriately substituted pyrazole moiety for maintaining antitubercular activity.

The SAR observations regarding the critical pharmacophoric features required for maintaining and/or improving antitubercular activity along with the scope for further SAR studies are summarized in Figure 3. In summary, the pyrimidin-4(3*H*)-one

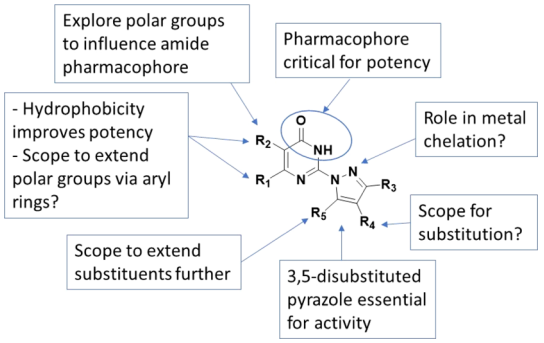

Figure 3. Essential pharmacophoric features and scope for further SAR studies.

ring was retained for further SAR studies considering the critical nature of the cyclic amide as well as the ring nitrogens for maintaining the antitubercular activity. The SAR observations suggest the important role of hydrophobic substituents at the R1 and R2 positions for potency. We explored the scope of polar interactions further away from the main scaffold by extending polar groups from the aryl ring at the R1 position. In addition, we also explored a few polar groups at the R2 position instead of a methyl group, which could influence HB-donor acceptor interactions of the pyrimidinone ring amide. The 3,5-disubstituted pyrazole ring was critical for maintaining activity, but there was a clear scope to extend substituents from the R5 position to improve potency and physicochemical properties. The scope of substitution at the R4-postion remained to be explored.

SAR of Polar Groups at R1 and R2 Positions of the Pyrimidinone Core. Several polar R1 and R2 substituents on the pyrimidinone ring were incorporated in order to expand the scope relative to activity (Table 3) and increase solubility and SI. Compound **19** with a 4-fluorophenyl group at the R1 position retained activity and cytotoxicity similar to compound **1**. The replacement of the phenyl ring with pyridine rings considerably improved solubility, as observed for compounds **20** and **21**, although with some loss in *Mtb* activity. Compound **20**, with a 4-pyridyl ring, was more potent (MIC 9 μM) than compound **21** with a 3-pyridyl ring (MIC 50 μM) leading to the speculation of the role of HB-interactions through the 4-pyridine nitrogen. Hence, compounds **22** to **25** with various polar substitutions at the para-position of the phenyl ring at the R1 position were prepared. Unfortunately, all these compounds lost activity. Next, we considered the option of inserting a polar linker between the pyrimidinone and phenyl rings. Among the various groups attempted, only compound **26** with a 4-flurophenyl group extended by a carboxamide linker at the R1 position, retained weak activity (25 μM).

Based on the encouraging data for compound **8** with a C5-methyl group on the pyrimidinone, we explored adding a few polar groups such as CN, $CONH_2$, and CO_2H at this position, but unfortunately this led to the loss of activity (compounds **27**, **28**, and **29**). Overall, these observations indicated very limited scope for adding polar substitutions on the pyrimidinone ring. Hence, we turned our attention to exploring possible interactions from the pyrazole ring.

SAR of the Pyrazole Ring. Further exploration on the pyrazole ring was planned, maintaining the CF_3 as the R1 substituent on the pyrimidinone, as it increased the solubility and SI exemplified for compound **12**. In addition, the smaller CF_3 group kept the molecular weight and lipophilicity on the low side compared to the phenyl. The addition of bulkier alkyls like ethyl and cyclopropyl (compounds **30** and **31**) at the R5 position on the pyrazole were tolerated for *Mtb* activity relative to **12** but with a deterioration of the SI, whereas a slight loss in activity was observed for compound **32** with the phenyl group at the R5 position. Isomers of these compounds with bulkier groups at the R3 position could not be synthesized because of the selectivity observed in the condensation reaction of hydrazine with requisite diketones favoring the placement of bulkier groups at the R5 position. Compound **33** with a NH_2 at the R5 position maintained a profile similar to compound **12**, whereas compound **34** with an aminoethyl at the R5 position showed increased toxicity against CHO cell lines without a significant improvement in activity. Compound **35** with an *O*-ethyl group at the R5 position had a potency and selectivity profile similar to compound **12**. The extension of polar groups like $-NH_2$ or $-OH$ via a short ethylamino linker from the R5 position as in compounds **36** and **37**, respectively, was detrimental to activity against *Mtb*. Compounds **38** and **39**, with the neutral ether substituents like methoxyethylamino and pyranamino, respectively, at the R5 position, showed more potent activity (MIC 1.5−2 μM) as compared to **12** while the SI was about the same. Based on these observations, it is speculated

https://dx.doi.org/10.1021/acs.jmedchem.0c01727
J. Med. Chem. 2021, 64, 719−740

Table 6. *In Vitro* ADME Properties of Selected Compounds[d]

compound	8	12	39	40	45	47	50
clog *P*[a]	1.82	1.36	1.30	2.52	1.46	0.66	1.54
clog *D*[a]	1.82	1.36	1.09	2.52	1.46	1.09	1.40
solubility (μM)[b]	120	200	50	15	25	90	160
MS[c] H/R/Mo % remaining after 30 min	65/54/45	>99/92/>99	>99/>99/93	98/98/96	>99/96/>99	80/95/94	ND
PPB[d] human *fu*	ND	0.006	0.014	0.013	ND	0.009	0.03

[a]Calculated log *P*/log *D* (StarDrop). [b]Kinetic solubility measured at pH 7.4. [c]Microsomal stability H: human, R: rat Mo: mouse. [d]PPB; *fu*—fraction unbound.

that the R5 position lies in a more hydrophobic region of the compound binding site within the target in *Mtb*. Hence, we decided to examine aryl groups, some with polarity, at R5 toward maintaining activity while improving solubility with polar substituents placed distant from the main scaffold.

Compound **40** with a 4-F-aniline at the R5 position showed *Mtb* potency and a SI profile similar to **39**, with an aminopyran at position R5, but had lower aqueous solubility (15 μM) as expected because of the overall increase in lipophilicity with an additional aryl ring. Compound **41** with a 2,4-difluoroanilino group at the R5 position was the most potent compound (MIC 0.2 μM) obtained so far in these studies but was poorly soluble (<5 μM) in aqueous media. The addition of polar groups like CN and dimethylcarboxamide (**42** and **43**) at the para-position of the R5-anilino groups decreased activity (MIC 9 and >50 μM, respectively). Similarly, compound **44** with a 4-pyridylamino at the R5 position was inactive against *Mtb* up to the highest concentration tested (MIC > 50 μM). Interestingly, compound **45** with a 2-pyridylamino group at the same R5 position was quite potent with a MIC of ≤1 μM. The compound had moderate aqueous solubility (25 μM) with a modest SI of 25 for CHO cell-line toxicity, thus making it a valuable compound for MoA studies (see below). A few compounds with polar substituents para to the amino group on the 2-pyridyl ring were synthesized and screened with a view to improving physicochemical properties. For example, compound **46** with a 4-morpholino-2-pyridylamino group at the R5 position retained good activity (MIC = 2 μM) with improved solubility (180 μM) but was significantly more cytotoxic (SI 0.6).

Compound **47**, with a 3-pyridyl at the R1 position and an ethylamino group at the R5 position, showed modest activity with an MIC of 6.25 μM and CHO IC_{50} of >50 μM.

A limited SAR exploration at the R4 position on the pyrazole was conducted to evaluate the scope for further improvement in potency and selectivity. Compound **48** with 4-bromopyrazole showed only moderate activity (MIC 25 μM, CHO IC_{50} > 50 μM) and was used as an intermediate for further synthesis. Replacing the bromine with a 3-pyridyl ring (**49**) abolished *Mtb* activity (MIC >50 μM), whereas the morpholine ring at this position (**50**) was well tolerated with an MIC = 6.25 μM and a cleaner cytotoxicity profile (CHO IC_{50} > 50 μM). In comparison, the R3 position on the pyrazole showed a very limited scope for further modifications. In general, a cyclopropyl group as in compound **51** was well tolerated for *Mtb* potency but larger groups in general gave weakly active compounds. Polar groups like dimethylaminomethyl, carboxylic acid, and amide as in compounds **52**, **53**, and **54**, respectively, led to considerable loss of activity against *Mtb* (MICs > 50 μM).

In summary, various modification on the pyrimidinone and pyrazole portions of the scaffold showed potential for improvement in potency against *Mtb in vitro* and MICs as low as 200 nM could be achieved. However, in general there was a narrow scope to improve the SI against mammalian cell-line toxicity. The potential impact of both these activities *in vivo* remains to be determined.

Physicochemical, DMPK, and Safety Profiles. Presented in Table 6 are physicochemical and *in vitro* DMPK properties of representative compounds, including solubility, microsomal MS, and human plasma protein binding (PPB). Compounds showed moderate to high aqueous solubility with excellent *in vitro* microsomal stability, with the exception of compound **8** that was only moderately stable in microsomes. A small number of compounds that were tested for the inhibition of liver cytochrome P450 enzymes did not show significant inhibition up to 20 μM (data not shown), indicating minimal possibility of metabolism-based drug−drug interactions of these compounds, which is a desirable attribute of a TB drug.[29,30] The compounds tested in the series were highly bound to the human plasma most likely due to the albumin binding of acidic pyrimidinone.[31] The safety profiles of compounds **1** and **12** were evaluated across a panel of 21 liability targets (39 functional assays), which included cell-based GPCRs and ion channels in both agonist and antagonist readout, and biochemical functional assays for nuclear hormone receptors and phosphodiesterases.[32] Both compounds showed no significant inhibition or activation of the enzyme/receptors at 10 μM test concentration. Both compounds showed hERG IC_{50} > 30 μM. In summary, the *in vitro* safety profile of the compounds indicated no obvious safety liability even though the reason for mammalian cytotoxicity observed was not clear.

The pharmacokinetic parameters of representative compounds, **12**, **47**, and **40** were measured from mouse blood at intravenous doses of 2 mg/kg and oral doses of 20 mg/kg in the mouse (Table 7). The compounds were well tolerated following either route of administration, with no obvious effects noted in the animals over the course of the exposure. Compounds **12** and **40** showed a low volume of distribution and low rate of clearance with moderate oral bioavailability of approximately 40%. Compound **47** showed rapid blood clearance and high volume of distribution with an oral bioavailability of 33%. Further analysis of mouse blood samples from the PK studies of **47** showed the glucuronide as the major metabolite. However, further optimization of physicochemical properties to improve pharmacokinetic properties, along with improved SI, is warranted in order to identify a compound suitable for *in vivo* efficacy studies in TB animal models.

Bactericidality and Activity against Clinical Isolates. The compounds were found to be bactericidal against replicating *Mtb* showing 2 log CFU reduction at 1−2× MIC over the time period of 7 days (Fig. S1). Importantly, we also evaluated the activity of **1**, **12**, **15**, and **20** against a panel of clinical isolates (Table S1). All the tested compounds retained MICs against clinical isolates within the 4-fold range of MICs against the drug-sensitive *Mtb* H37Rv strain.

https://dx.doi.org/10.1021/acs.jmedchem.0c01727
J. Med. Chem. 2021, 64, 719−740

Table 7. Pharmacokinetic Parameters in Male C57/BL6 Mouse Blood[a]

route of administration	i.v.	oral	i.v.	oral	i.v.	oral
	12		**47**		**40**	
dose (mg/kg)	2	20	2	20	2	20
apparent $t_{1/2}$ (h)	3.1	4	5.6	4.4	4.0	6.1
CL_{total} (mL/min/kg)	2.7		80.9		0.4	
CL_{int} (mL/min/kg)	476		>4000		34	
V_d (L/kg)	0.7		37.4		0.1	
C_{max} (μM)	29.1	65.6	2.4	2.9	33.1	104.5
T_{max} (h)		0.5		0.5		1.0
$AUC_{0-\infty}$ (min·μM)	2928	12004	91	313	15373	65417
oral bioavailability F (%)		41		33		44

[a]i.v.: intravenous; $t_{1/2}$: elimination half-life; CL_{total}: total blood clearance; CL_{int}: intrinsic clearance; V_d: volume of distribution during elimination phase; C_{max}, maximum (peak) plasma concentration following oral administration; and AUC: area under the curve.

Target Deconvolution Studies. *Biology Triaging.* In order to explore the MoA, potent compounds were initially screened against various tool strains to rule out the involvement of known mechanisms and/or targets. The tested compounds retained activity against a QcrB mutant (A396T) and did not show hypersensitivity against a cytochrome-bd oxidase knockout mutant strain (*cyd*KO),[33] thereby eliminating them as potential targets. The compounds did not show a positive signal in two standard bioluminescence reporter assays: PiniB-LUX[34]—detects modulation in the *iniB* expression, if a compound targets *Mtb* cell−wall biosynthesis, and PrecA-LUX[34]—detects modulation in the *recA* expression, an indicator of genotoxic compounds. A strain carrying a mutation in DprE1 (C387S), which confers resistance to other DprE1 inhibitors, was not resistant, suggesting DprE1 is not the target. However, strains carrying mutations in MmpL3 were cross-resistant to compounds (Table 8).[35] The compounds showed an increase of

Table 8. Cross-Screening against mmpL3 Mutants[a]

strain	**1**	**2**	**12**	**15**	**47**	**40**	**38**
H37Rv WT MIC (μM)	1.7	4.8	15	27	5.8	1.2	1.2
MmpL3 F255L MIC (μM)	18	55	170	>200	41	>200	39
MmpL3 F644L MIC (μM)	1.9	5.4	17	24	5.5	1	1.9
MmpL3 V681 MIC (μM)	16	45		>200			
MmpL3 G596R MIC (μM)	40	110		>200			

[a]WT: wild-type.

8−100-fold in MIC values against the strains with either $MmpL3_{F255L}$ or $MmpL3_{V681I}$ or $MmpL3_{G596R}$, whereas, there was no change in activity against the $MmpL3_{F644L}$ mutant. Most of these mutations lie within the region required for proton translocation.[36] Variability in the MICs against these mutant strains is suggestive of the fact that the compounds may bind differently to the protein depending on the mutation. To investigate whether or not compounds **1**, **2**, **12**, **15**, **47**, **40**, and **38** retain target selectivity for MmpL3 in *Mtb* cells, we asked whether or not conditional depletion of MmpL3 in a *mmpL3* hypomorph (Grover et al., manuscript under review) would sensitize *Mtb* to the growth inhibitory effects of the compounds. However, transcriptional silencing of *mmpL3* resulted in no significant change in the MICs of the compounds, confirming that MmpL3 is not the direct target of this series (Table S2). We hypothesize that MmpL3 acts as a transporter of these compounds across the cell membrane as the compounds can form heme-like iron-complexes, and MmpL3 is known to act as a heme transporter.[37,38] Hence, MmpL3 is likely to be responsible for building resistance toward compounds through the impairment of transport of compounds across the cell membrane rather than being a direct target. It is to be noted that the compounds were PiniB-LUX negative—indicating a non-cell wall MoA.

Based on the structural similarity of the compounds with the published thymidylate kinase inhibitors,[39,40] we asked whether this compound series can inhibit *Mtb* thymidylate kinase, which is an essential target encoded by Rv3247c. To investigate this, we tested the activity of the compounds **1**, **2**, and **12** against the Rv3247c hypomorph. However, we did not observe any MIC modulation of the compounds upon silencing of Rv3247c, suggesting that the tested compounds are not the thymidylate kinase inhibitors.

*Treatment with **45** and **12** Affects Genes Involved in Fe Homeostasis.* In continuation of our efforts to explore MoA, the effects of **45** (at 1 μM and 10 μM) and **12** (at 20 μM) treatment on the gene expression of *Mtb* was investigated. *Mtb* cultures were treated with the compound for 6 h, harvested, and the RNA extracted for transcriptional profiling by microarray analysis. The data obtained from the transcriptional profiling of *Mtb* exposed to **45** and **12** were similar (Table S3). We performed in-depth analysis of the data obtained from samples treated with **45**, which was tested at two concentrations. The 50 most upregulated (>4-fold) genes were selected in order to understand their potential contribution in the cellular response based on the MoA of **45** (Table S4). This indicated a transcriptional signature related to iron-sequestration. The upregulated genes included *rv2377c-78c-79c-80c-81c-82c-83c-84-85-2386c* (*mbtA-H*)—all of which are associated with mycobactin biosynthesis or regulation,[41] which are known to be upregulated in response to iron deprivation.

Another upregulated gene-set *rv1342-43-44-45-46-47-48-49* is also associated with the mycobactin biosynthesis or regulation or with iron transport where *rv1348* and *rv1349* were annotated as iron-regulated transporters, both being essential for growth *in vitro*.[42−44] The *esx-3* gene cluster is composed of 11 genes stretching from *rv0282* to *rv0292*. All of these were upregulated 2−5-fold in response to the stress caused by the compound. *rv0287* and *rv0288* are predicted to be essential for growth *in vitro*. Interestingly, ESX-3 is known to be required for the mycobactin-mediated siderophore iron uptake pathway,[45−48] and it is essential in *Mtb* but not in *Mycobacterium smegmatis*, a species which, in addition to mycobactins, produces exochelin that functions independently of ESX-3. However, ESX-3 is still required for mycobactin-mediated iron uptake in the latter species.[45,46,48] The nonessential nature of ESX-3 in *M. smegmatis* has previously proven to be of a great advantage when resolving mechanisms related to ESX-3 and mycobactin iron metabolism.[48] Some of the top upregulated genes are involved in lipid

https://dx.doi.org/10.1021/acs.jmedchem.0c01727
J. Med. Chem. 2021, 64, 719−740

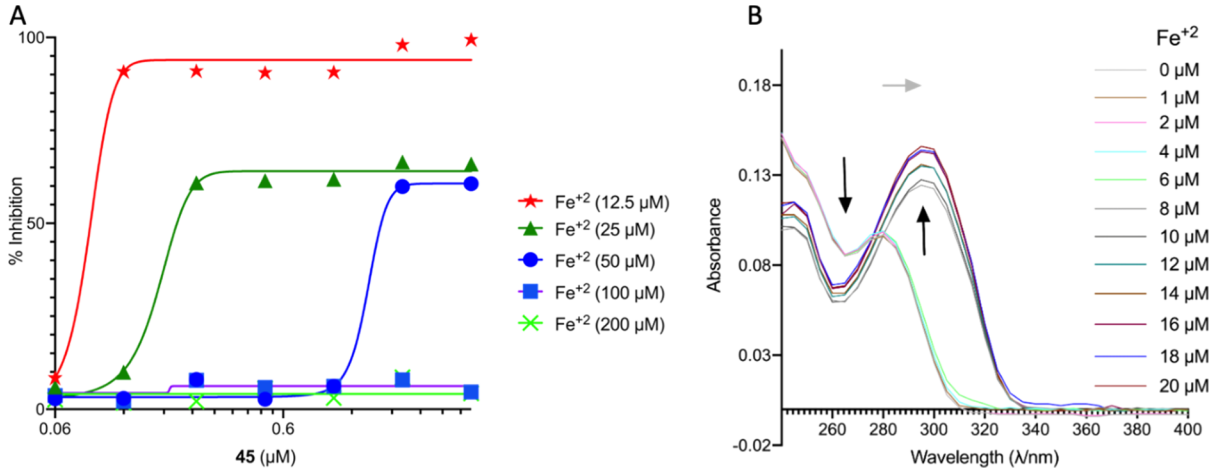

Figure 4. Fe^{2+} plays a critical role in the MoA of **45**. (A) Fe^{2+} rescue of *Mtb* from growth inhibition mediated by **45**. (B) Spectroscopic titration of **45** with Fe^{2+}. The data are representative of two biological replicates performed in duplicate.

metabolism, for example, *rv3249-51-52* potentially a transcriptional response to correct damage to fatty acids. Fe has been reported to affect lipid metabolism, specifically because of Fe-catalyzed lipid oxidation. In line with this, we observed that genes, including *rv3741-42*, (oxidoreductase) were upregulated. The observed upregulation of the *rv3269-70* operon encoding a stress response protein and a metal cation transporter, respectively, further supports the notion that the cellular response to **45** is one of the disruption of iron homeostasis. R*v0285*—PE5 which was upregulated in our study, is downregulated in the presence of iron.[49] Importantly, most of the upregulated genes of our data set were found to be downregulated when *Mtb* was exposed to an excess of iron.[49] Our data set also complements the recently published work by Kurthkoti et al.,[50] where authors performed transcriptomics in iron-starved cultures and identified similar upregulated clusters of genes. This strongly suggests that the disruption of Fe homeostasis is an important component of the MoA of **45**.

In summary, our data suggest that upon exposure to 2-pyrazolylpyrimidinones, *Mtb* goes into an iron-starvation state. As expected, it upregulates genes involved in the mycobactin (siderophore) synthesis pathway and its regulation. Siderophores are small, high-affinity iron-chelating compounds secreted by microorganisms such as bacteria and fungi. In the process of cellular uptake, the Fe^{3+}-siderophore complex is subsequently reduced to Fe^{2+} to release the iron.

Iron Plays a Significant Role in the MoA. To confirm the role of iron in the MoA of this series, an Fe rescue experiment was performed by supplementing standard Middlebrook 7H9/Glu/CAS/Tx media with 200 μM ferric ammonium citrate. The supplementation of Fe^{3+} resulted in a 4-fold increase in the MIC (Table S5). Under physiological conditions, iron can exist in either the reduced ferrous (Fe^{2+}) form or the oxidized ferric (Fe^{3+}) form. The redox potential of Fe^{2+}/Fe^{3+} makes iron extremely versatile when it is incorporated into proteins as a catalytic center or as an electron carrier. Thus, iron is important for numerous biological processes, which include the tricarboxylic acid cycle, gene regulation, DNA biosynthesis, and so forth. Although iron is abundant in nature, it does not normally occur in its biologically relevant but aerobically unstable ferrous form. To evaluate this, we supplemented the *Mtb* culture with 200 μM ferrous sulfate, resulting in an 8-fold increase in the MIC for **45** (Table S5). Next, we confirmed the ability of Fe^{2+} to rescue the *Mtb* from **45** toxicity in a checkerboard (2D) assay using GAST (glycerol-alanine-salts-Tween 80) media which is devoid of Fe unlike Middlebrook 7H9/Glu/CAS/Tx (Figure 4A). The inhibition of *Mtb* growth by **45** in GAST medium supplemented with 12.5 μM Fe^{+2} (MIC 0.12 μM) decreased in a dose-dependent manner with increasing concentration of Fe^{2+} and resulted in a ≥32-fold increase in MIC at 100/200 μM Fe^{2+}. To determine that **45** forms a complex with Fe^{2+}, we performed UV−vis scanning of **45** with increasing amounts of Fe^{2+} (Figure 4B). The band intensity at 270, which was observed for **45** alone, decreased after the addition of Fe^{2+}, whereas the absorbance around 285 is shifted to 300 with the increase in intensity, indicating the formation of the **45**-Fe^{2+} complex.

In line with the observation of better rescue with ferrous than ferric iron and a preference of heme for the former, there is a strong possibility that the compound binds iron to form a heme-like complex that enters *Mtb* via MmpL3. This also supports the reason for resistance with some of the MmpL3 mutants as described previously—heme prefers ferrous over ferric. Involvement of a heme-like structure could also explain the associated cytotoxicity of the series, as described earlier. This is because of the toxic nature of heme to eukaryotic cells, which require specific heme-binding proteins to maintain a nontoxic homeostasis.

CONCLUSIONS

Whole-cell phenotypic screening of MMV compound library led to the identification of 2-pyrazolylpyrimidinones with potent antitubercular activity and a novel mode of action. Detailed SAR studies identified several compounds with potent activity against *Mtb* with moderate to high aqueous solubility and excellent *in vitro* microsomal stability. The compounds were bactericidal against replicating *Mtb* and retained potency against clinical isolates. Transcriptional profiling suggested that upon exposure to 2-pyrazolylpyrimidinones, *Mtb* goes into an iron-starvation state that may account for lethality. Iron supplementation using a high concentration of ferrous salts showed shifts in MICs of the compounds, further confirming that 2-pyrazolylpyrimidinones perturbs the Fe-homeostasis in *Mtb*. Further optimization of pharmacokinetic properties, along with improved SI between MIC and mammalian cytotoxicity, is needed to identify a compound suitable for *in vivo* efficacy studies in mouse TB

https://dx.doi.org/10.1021/acs.jmedchem.0c01727
J. Med. Chem. 2021, 64, 719−740

models and eventual development as a viable drug useful for the treatment of TB in humans.

EXPERIMENTAL SECTION

MIC Testing and Triage Assays. Unless otherwise indicated, an Alamar Blue fluorescence-based broth microdilution assay was used to assess MIC of compounds against *Mtb* strains, as described previously.[51,52] Rifampicin was included as a control. Biology triage assays were carried out as described by Naran et al.[34]

MICs against Mutant Strains. MICs were determined after 5 days of growth in Middlebrook 7H9 medium plus OADC supplement and 0.05% w/v Tween 80 as described previously.[53] Growth was monitored by OD. Data were fit using the Levenberg−Marquardt least-squares plot. MIC was defined as the concentration required to inhibit growth by 90%.

RNA Extraction and Transcriptional Profiling. Total RNA was extracted from *Mtb* H37Rv that had been treated for 6 h with 1× and 10× MIC of the compound or vehicle control as previously described.[54] RNA quality was confirmed by UV spectral analysis and Agilent 2100 Bioanalyzer returning a RNA integrity number of 8 or higher. Fluorescent-tagged cDNA was prepared via a direct random-primed labeling method as follows. To 4.0 μg of RNA, 4.5 μg of a random hexamer (Invitrogen# 48190-011) was added, a final volume of 14.5 μL, heat denatured at 70 °C for 5 min then immediately cooled to 0 °C on ice. cDNA synthesis and fluorophore (Cy3 or Cy5) incorporation were carried out using the following reverse transcription reaction components 5 μL of 5× First-Strand buffer, 1.25 μL of 0.1 M DTT, 2.5 μL of dNTP mix (made by 5 mM each of dATP, dGTP), dTTP, 0.5 mM dCTP, plus 1 μL of 200 U/μL SuperScriptIII (Invitrogen# 18080-044), 1 μL of 40 U/μL RNAseOut, and 1 μL of Cy3 or Cy5-dCTP (GE# PA55321) were added for incubation at 25 °C for 5 min and at 48 °C for 90 min. Template RNA was chemically hydrolyzed by 5 μL of 1 M NaOH and heated at 70 °C for 15 min. The hydrolysis reaction was neutralized with 5 μL of 1 M HCl. The labeled cDNA was purified on an Amicon Ultra-0.5 column (Millipor# C82301) following the manufacturer's recommendations for PCR purification. cDNA yields and dye incorporation were measured with a Nanodrop ND-1000. A mixture of equal amounts (0.7 μg) of Cy3- and Cy5-labeled cDNA was loaded into hybridization chambers for incubation with an Agilent SurePrint G3 4x44K custom oligonuclotide microarray (design number 021966, 021362).

Microarrays were hybridized robotically using a TECAN HS Pro 4800 hybridization station, Agilent 2× gene expression hybridization HI-RPM buffer, and 10× blocking reagent at 65 °C for 17 h and washed with Agilent Gene Expression Wash Buffer 1 at room temperature and Gene Expression Wash Buffer 2 at 37 °C. Then, slides were dried under a nitrogen gas for 3 min at 30 °C. The slides were imaged using an Agilent high-resolution DNA microarray scanner (model G2505C) at 5 μm resolution and 100/10% PMT dual scanning for XDR extended dynamic range. Agilent Feature Extraction software was used for image analysis.

DMPK. All protocols for *in vitro* DMPK studies and mouse PK studies are available in the supplementary document. Animal studies were conducted following guidelines and policies as stipulated in the UCT Research Ethics Code for Use of Animals in Research and Teaching, after review and approval of the experimental protocol by the UCT Senate Animal Ethics Committee (protocol FHS-AEC 013/032).

Chemistry. All commercial reagents were purchased from Sigma-Aldrich, Combi-Blocks, Enamine, or Fluorochem and were used without further purification. Solvents were used as received unless otherwise stated. Analytical thin-layer chromatography was performed on SiO2 plates on aluminum backing. Visualization was accomplished by UV irradiation at 254 and 220 nm. Flash column chromatography was performed using a Teledyne ISCO flash purification system with SiO_2 60 (particle size 0.040−0.055 mm, 230−400 mesh). Purity of all final derivatives for biological testing was confirmed to be >95% as determined using an Agilent 1260 Infinity binary pump, Agilent 1260 Infinity diode array detector (DAD), Agilent 1290 Infinity column compartment, Agilent 1260 Infinity standard autosampler, and Agilent 6120 quadrupole (single) mass spectrometer, equipped with APCI and ESI multimode ionization sources. Using a Kinetex Core C18 2.6 μm column (50 mm × 3 mm); mobile phase B of 0.4% acetic acid, 10 mM ammonium acetate in a 9:1 ratio of HPLC grade methanol and type 1 water, mobile phase A of 0.4% acetic acid in 10 mM ammonium acetate in HPLC grade (type 1) water, with a flow rate of 0.9 mL/min, DAD; or an Agilent UPLC−MS was used: Agilent Technologies 6150 quadrupole, ES ionization, coupled with an Agilent Technologies 1290 Infinity II series UPLC system Agilent 1290 series HPLC at two wavelengths 254 and 290 nm using the following conditions: Kinetex 1.7 μm Evo C18 100A, LC column 50 mm × 2.1 mm, solvent A of 0.1% (formic acid) water, and solvent B of 0.1% (formic acid) acetonitrile. The structures of the intermediates and end products were confirmed by ^{1}H NMR and mass spectrometry. Proton magnetic resonance spectra were determined in an appropriate deuterated solvent on a Varian Mercury spectrometer at 300 MHz or a Varian Unity spectrometer at 400 MHz.

*2-(3,5-Dimethyl-1H-pyrazol-1-yl)-6-phenylpyrimidin-4(3H)-one (**1**).* A mixture of 2-hydrazinyl-6-phenylpyrimidin-4(3*H*)-one (**56a** 0.2 g, 0.989 mmol) and pentane-2,4-dione (0.121 mL, 1.187 mmol) was heated in a mixture of ethanol (0.5 mL) and acetic acid (1.5 ml) at 100 °C for 16 h. After cooling to room temperature, the reaction mixture was poured into ice cooled water and stirred for 30 min. Solids formed were filtered, washed with water, and dried to yield **1** as a white solid (200 mg, 0.744 mmol, 75% yield). HPLC purity: >99%. LC−MS APCI: calcd for $C_{15}H_{14}N_4O$, 266.304; observed m/z $[M + H]^+$, 267.1. ^{1}H NMR (300 MHz, $CDCl_3$): δ 8.01−7.97 (m, 2H), 7.53−7.50 (m, 3H), 6.73 (s, 1H), 6.12 (s, 1H), 2.55 (s, 3H), 2.32 (s, 3H).

*6-Methyl-2-(3-methyl-5-(p-tolylamino)-1H-pyrazol-1-yl)-pyrimidin-4(3H)-one (**2**).* Compound was received from the MMV screening library. For synthesis and analytical data, please refer WO2012154880.[2]

*2-(3,5-Dimethyl-1H-pyrazol-1-yl)-4-methoxy-6-phenylpyrimidine (**3**).* DIAD (0.110 mL, 0.563 mmol) was added dropwise to a solution of 2-(3,5-dimethyl-1*H*-pyrazol-1-yl)-6-phenylpyrimidin-4(3*H*)-one (**1**) (100 mg, 0.376 mmol), triphenylphosphine (148 mg, 0.563 mmol) in methanol (12.03 mg, 0.376 mmol), and tetrahydrofuran (100 mL), and the reaction mixture was stirred at room temperature for 4 h. The mixture was concentrated under reduced pressure, the residue partitioned between dichloromethane and water, and the layers separated. The aqueous phase was extracted with dichloromethane, the combined organic solutions washed consecutively with water, 2 N aqueous sodium hydroxide, water, and finally brine. The solution was then dried over sodium sulfate and evaporated under reduced pressure. The crude product was purified on an ISCO system using a 4 g silicycle column and eluting with a gradient 0 to 70% ethyl acetate in hexane over 20 min to yield **3** as a white solid (27 mg, 0.09 mmol, 24% yield). HPLC purity: 95%. LC−MS APCI: calcd for $C_{16}H_{16}N_4O$, 280.33; observed m/z $[M + H]^+$, 281.1. ^{1}H NMR (300 MHz, $CDCl_3$): δ 7.99−7.96 (m, 2H), 7.49−7.47 (m, 3H), 6.92 (s, 1H), 6.31 (br s, 1H), 6.08 (s, 1H), 3.56 (s, 3H), 2.50 (s, 3H), 2.33 (s, 3H).

*2-(3,5-Dimethyl-1H-pyrazol-1-yl)-3-methyl-6-phenylpyrimidin-4(3H)-one (**4**).* To a stirred solution of 2-(3,5-dimethyl-1*H*-pyrazol-1-yl)-6-phenylpyrimidin-4(3*H*)-one (**1**) (50 mg, 0.188 mmol) in DMF (2 mL) was added potassium carbonate (52 mg, 0.563 mmol). The reaction mixture was stirred for 5 min and iodomethane (35 μL, 0.563 mmol) was added. The reaction mixture was stirred at 100 °C overnight. The reaction mixture was extracted with ethyl acetate (3 × 10 mL). The combined organic layer was washed with LiCl solution (1 × 10 mL) and dried over sodium sulfate, and the solvent was evaporated. The obtained residue was purified by flash chromatography by using 15% ethyl acetate in hexane obtained **4** as a white solid (39 mg, 0.141 mmol, 75% yield). HPLC Purity: 96%. LC−MS APCI: calcd for $C1_6H_{16}N_4O$, 280.33; observed m/z $[M + H]^+$, 281.1. ^{1}H NMR (300 MHz, $CDCl_3$): δ 8.01−7.97 (m, 2H), 7.53−7.50 (m, 3H), 6.73 (s, 1H), 6.18 (s, 1H), 3.52 (s, 3H), 2.55 (s, 3H), 2.32 (s, 3H).

*6-(3,5-Dimethyl-1H-pyrazol-1-yl)-4-phenylpyridin-2(1H)-one (**5**).* To a cooled solution of crude **61** (0.40 g, 1.43 mmol) in methanol (7 mL) was added boron tribromide (1 M solution in dichloromethane) (4.2 mL, 4.29 mmol) and stirred for 16 h at room temperature. Water

https://dx.doi.org/10.1021/acs.jmedchem.0c01727
J. Med. Chem. 2021, 64, 719−740

was added to the reaction mixture and extracted with dichloromethane. The combined organic phase was dried over sodium sulfate, concentrated under vacuum, and purified by preparative HPLC to give **5** as a white solid (0.08 g, 21%). HPLC purity: 98.6%. LC−MS APCI: calcd for $C_{16}H_{15}N_3O$, 265.122; observed m/z $[M + H]^+$, 266.2. ^1H NMR (400 MHz, $CDCl_3$): δ 9.38 (br s, 1H), 7.64−7.62 (m, 2H), 7.51−7.47 (m, 3H), 6.76 (s, 1H), 6.70 (s, 1H), 6.07 (s, 1H), 2.58 (s, 3H), 2.3 (s, 3H).

*2-(3,5-Dimethyl-1H-pyrazol-1-yl)-6-phenylpyridin-4(1H)-one (**6**).* Synthesized from intermediate **62** with a protocol similar to the one described for compound **5**. Yield 25% (white solid); HPLC purity: 98.9%. LC−MS APCI: calcd for $C_{16}H_{15}N_3O$, 265.122; observed m/z $[M + H]^+$, 266.2. ^1H NMR (400 MHz, $CDCl_3$): δ 10.49 (br s, 1H), 7.96 (d, J = 6.4 Hz, 2H), 7.46−7.40 (m, 4H), 7.11 (s, 1H), 6.07 (s, 1H), 2.70 (s, 3H), 2.35 (s, 3H).

*6-(3,5-Dimethyl-1H-pyrazol-1-yl)-4-phenylpyrimidin-2(1H)-one (**7**).* To the solution of 2-chloro-4-(3,5-dimethyl-1*H*-pyrazol-1-yl)-6-phenylpyrimidine (intermediate **65**, 0.16 g, 0.56 mmol) in THF (2 mL) was added 2 M aqueous NaOH solution (2 mL) at room temperature, and the mixture was heated at 80 °C for 4 h. The reaction mixture was then cooled in ice-bath and acidified with glacial acetic acid. The precipitated solid was filtered under vacuum, washed with chilled water, and dried to get 6-(3,5-dimethyl-1*H*-pyrazol-1-yl)-4-phenylpyrimidin-2(1*H*)-one (7, 0.12 g, 80% yield) as a white crystalline powder. HPLC purity: 99.2%. LC−MS APCI: calcd for $C_{15}H_{14}N_4O$, 266.117; observed m/z $[M + H]^+$, 267.2. ^1H NMR (400 MHz, DMSO-d_6): δ 8.11 (m, 2H), 7.53 (m, 3H), 6.92 (s, 1H), 6.26 (s, 1H), 2.71 (s, 3H), 2.23 (s, 3H).

*2-(3,5-Dimethyl-1H-pyrazol-1-yl)-5-methyl-6-phenylpyrimidin-4(3H)-one (**8**).* Synthesized from intermediate **56b** following a protocol similar to compound **1**. Yield 10% (white solid). HPLC purity: 97%. LC−MS APCI: calcd for $C_{16}H_{16}N_4O$, 280.331; observed m/z $[M + H]^+$, 281.1. ^1H NMR (300 MHz, $CDCl_3$): δ 7.68−7.58 (m, 2H), 7.55−7.39 (m, 3H), 6.05 (s, 1H), 2.69 (s, 3H), 2.30 (s, 3H), 2.19 (s, 3H).

*2-(3,5-Dimethyl-1H-pyrazol-1-yl)-6-methyl-5-phenylpyrimidin-4(3H)-one (**9**).* Synthesized from intermediate **56h** following a protocol similar to compound **1**. Yield 10% (white solid). HPLC purity: 98.9%. LC−MS APCI: calcd for $C_{16}H_{16}N_4O$, 280.132; observed m/z $[M + H]^+$, 281.0. ^1H NMR (400 MHz, $CDCl_3$): δ 10.59 (s, 1H), 7.27−7.44 (m, 5H), 6.05 (s, 1H), 2.71 (s, 3H), 2.26 (s, 3H), 2.22 (s, 3H). ^{13}C NMR (100 MHz, $CDCl_3$): 13.63, 15.08, 22.99, 111.38, 122.18, 127.70, 128.36, 130.17, 133.72, 143.40, 145.66, 151.82, 161.01, 161.19.

*2-(3,5-Dimethyl-1H-pyrazol-1-yl)quinazolin-4(3H)-one (**10**).* Synthesized from 2-hydrazineylquinazolin-4(3*H*)-one following a protocol similar to compound **1**. Yield 47% (white solid). HPLC purity: 96.3%. LC−MS APCI: calcd for $C_{13}H_{12}N_4O$, 240.10; observed m/z $[M + H]^+$, 241.1. ^1H NMR (400 MHz, DMSO-d_6): δ 11.92 (s, 1H), 8.11 (dd, J = 7.9, 1.5 Hz, 1H), 7.81 (ddd, J = 8.5, 7.2, 1.6 Hz, 1H), 7.65 (d, J = 8.1 Hz, 1H), 7.53−7.43 (m, 1H), 6.27 (s, 1H), 2.69 (s, 3H), 2.26 (s, 3H). ^{13}C NMR (101 MHz, DMSO-d_6): δ 160.68, 151.04, 147.19, 143.23, 139.59, 135.19, 126.65, 126.46, 118.79, 115.59, 111.34, 14.74, 13.85.

*2-(3,5-Dimethyl-1H-pyrazol-1-yl)-6-methylpyrimidin-4(3H)-one (**11**).* Synthesized from intermediate **56c** following a protocol similar to compound **1**. Yield 78% (white solid). HPLC purity: 96%. LC−MS APCI: calcd for $C_{10}H_{12}N_4O$, 204.23; observed m/z $[M + H]^+$, 205.1 ^1H NMR (300 MHz, $CDCl_3$): δ 6.73 (s, 1H), 6.12 (d, 1H), 2.55 (s, 3H), 2.32 (s, 3H), 2.23 (d, 1H).

*2-(3,5-Dimethyl-1H-pyrazol-1-yl)-6-(trifluoromethyl)pyrimidin-4(3H)-one (**12**).* Synthesized from intermediate **56d** following a protocol similar to compound **1**. Yield 70% (white solid). HPLC purity: 98.9%. LC−MS APCI: calcd for $C_{10}H_9F_3N_4O$, 258.07; observed m/z $[M + H]^+$, 259.0. ^1H NMR (400 MHz, DMSO-d_6): δ 6.79 (s, 1H), 6.27 (s, 1H), 2.56 (s, 3H), 2.23 (s, 3H). ^{13}C NMR (100 MHz, DMSO-d_6): δ 13.83, 14.77, 111.89, 119.62, 122.34, 143.71, 152.04.

*2-(3-Methyl-5-oxo-2,5-dihydro-1H-pyrazol-1-yl)-6-phenylpyrimidin-4(1H)-one (**13**).* A mixture of 2-hydrazineyl-6-phenylpyrimidin-4(1*H*)-one (**56a**, 150 mg, 0.742 mmol) and ethyl acetoacetate (0.114 mL, 0.890 mmol) was heated in a mixture of ethanol: acetic acid, 1:3, under reflux for 5 h. The solid product obtained after cooling and pouring onto ice-cold water was filtered off, washed with water, and crystallized from ethanol to give **13** as a white solid (39 mg, 0.148 mmol, 20% yield). HPLC purity 93%. LC−MS APCI: calcd for $C_{14}H_{12}N_4O_2$, 268.27; observed m/z $[M + H]^+$, 269.1. ^1H NMR (400 MHz, DMSO-d_6): δ 8.22−8.20 (m, 2H), 7.54−7.51 (m, 2H), 6.74 (s, 1H), 5.31 (s, 1H), 2.29 (s, 3H).

*2-(5-Amino-3-methyl-1H-pyrazol-1-yl)-6-phenylpyrimidin-4(1H)-one (**14**).* 2-Hydrazineyl-6-phenylpyrimidin-4(1*H*)-one **56a** (0.1 g, 0.495 mmol) and 3-aminocrotonitrile (0.042 g, 0.519 mmol) were stirred in ethanol (5 mL) and refluxed for 5 h. The solvent was removed, and the crude product was recrystallized from methanol to afford **14** as a white solid (55 mg, 0.742 mmol, 42% yield). HPLC purity: 97%. LC−MS APCI: calcd for $C_{14}H_{13}N_5O$, 267.29; observed m/z $[M + H]^+$, 268.1. ^1H NMR (300 MHz, DMSO-d_6): δ 8.04−7.92 (m, 2H), 7.60−7.49 (m, 3H), 6.91 (s, 2H), 6.73 (s, 1H), 5.35 (s, 1H), 2.13 (s, 3H). ^{13}C NMR (101 MHz, DMSO-d_6): δ 192.03, 152.67, 151.14, 136.44, 131.20, 129.40, 127.22, 89.28, 14.37.

*N-(3-Methyl-1-(4-oxo-6-phenyl-1,4-dihydropyrimidin-2-yl)-1H-pyrazol-5-yl)acetamide (**15**).* A mixture of 2-(5-amino-3-methyl-1*H*-pyrazol-1-yl)-6-phenylpyrimidin-4(1*H*)-one (**14**, 100 mg, 0.374 mmol) and pyridine (0.04 mL, 0.442 mmol) in dichloromethane (2 mL) was treated with a solution of acetyl chloride (0.04 mL, 0.0448 mmol) in dichloromethane (1 mL). The reaction mixture was stirred at room temperature for 24 h before it was diluted with dichloromethane (5 mL). The mixture was washed with 2 N HCl (10 mL), 5% aqueous solution of $NaHCO_3$, and brine. The organic phase was dried over sodium sulfate, filtered, and concentrated *in vacuo* to give **15** as a white solid (45 mg, 0.145 mmol, 39% yield). HPLC purity: 98%. LC−MS APCI: calcd for $C_{16}H_{15}N_5O_2$, 309.33; observed m/z $[M + H]^+$, 310.1. ^1H NMR (300 MHz, DMSO-d_6): δ 11.55 (s, 1H), 8.13−8.03 (m, 2H), 7.63−7.52 (m, 3H), 6.95 (s, 1H), 6.64 (s, 1H), 2.22 (d, J = 15.1 Hz, 6H).

*6-Phenyl-2-(1H-pyrazol-1-yl)pyrimidin-4(3H)-one (**16**).* In a 10 mL microwave vial, 2-chloro-6-phenylpyrimidin-4(3*H*)-one (**66**, 0.1 g, 0.484 mmol), 1*H*-pyrazole (0.066 g, 0.968 mmol), and cesium carbonate (0.473 g, 1.452 mmol) were mixed in 1,4-dioxane (1 mL). The vial was capped and microwaved at 100 °C for 1 h. LCMS indicated two products of the same mass (isomers from 70:30 ratio of the starting material). The reaction mixture was concentrated and purified by preparative HPLC to afford **16** as a white solid (29 mg, 0.121 mmol, 25% yield). HPLC purity: 96%. LC−MS APCI: calcd for $C_{13}H_{10}N_4O$, 238.25; observed m/z $[M + H]^+$, 239.1. ^1H NMR (300 MHz, DMSO-d_6): δ 8.78 (d, 1H, J = 3 Hz), 8.24−8.20 (m, 2H), 7.89 (d, 1H, J = 1.2 Hz), 7.56−7.53 (m, 3H), 7.07 (s, 1H), 6.65 (dd, 1H, J = 3 and 1.8 Hz).

*2-(3,5-Dimethyl-1H-1,2,4-triazol-1-yl)-6-phenylpyrimidin-4(3H)-one (**17**).* Synthesized from intermediate **66** and 3,5-dimethyl-1*H*-1,2,4-triazole following a protocol similar to compound **16**. Yield 28% (white solid). HPLC purity: 99%. LC−MS APCI: calcd for $C_{14}H_{13}N_5O$, 267.29; observed m/z $[M + H]^+$, 268.1. ^1H NMR (300 MHz, DMSO-d_6): δ 7.95−7.93 (m, 2H), 7.63−7.57 (m, 3H), 7.22 (s, 1H), 2.80 (s, 3H), 2.32 (s, 3H).

*2-(1-Methyl-1H-imidazole-2-yl)-6-phenylpyrimidin-4(1H)-one (**18**).* 1-methyl-1*H*-imidazole-2-carboximidamide (0.075 g, 0.61 mmol) and ethyl benzoylacetate (0.12 g, 0.61 mmol) were refluxed in EtOH for 2 h. The reaction was cooled, solvent was evaporated under vacuo, and the residue was purified on preparative HPLC to give 2-(1-methyl-1*H*-imidazol-2-yl)-6-phenylpyrimidin-4(1*H*)-one (**18**, 15 mg, Yield 10%) as a brown solid. HPLC purity: 94.2%. LC−MS APCI: calcd for $C_{14}H_{12}N_4O$, 252.101; observed m/z $[M + H]^+$, 253.4, ^1H NMR (400 MHz, DMSO-d_6): δ 7.99 (t, J = 3.6 Hz, 2H), 7.52−7.49 (m, 3H), 7.21 (s, 1H), 7.14 (s, 1H), 6.83 (s, 1H), 4.29 (s, 3H).

*2-(3,5-Dimethyl-1H-pyrazol-1-yl)-6-(4-fluorophenyl)pyrimidin-4(3H)-one (**19**).* Synthesized from intermediate **56e** following a protocol similar to compound **1**. Yield 33% (white solid). HPLC purity: 93%. LC−MS APCI: calcd for $C_{15}H_{13}FN_4O$, 284.29; observed m/z $[M + H]^+$, 285.1. ^1H NMR (300 MHz, DMSO-d_6): δ 8.18−8.14 (m, 2H), 7.58−7.32 (m, 2H), 6.89 (s, 1H), 6.26 (s, 1H), 2.71 (s, 3H), 2.24 (s, 3H), 2.09 (br s, 1H).

*2-(3,5-Dimethyl-1H-pyrazol-1-yl)-6-(pyridin-4-yl)pyrimidin-4(3H)-one (**20**).* Synthesized from intermediate **56f** following a protocol similar to compound **1**. Yield 45% (white solid). HPLC

https://dx.doi.org/10.1021/acs.jmedchem.0c01727
J. Med. Chem. 2021, 64, 719−740

purity: 96%. LC−MS APCI: calcd for $C_{14}H_{13}N_5O$, 267.29; observed m/z $[M + H]^+$, 268.1. ^1H NMR (300 MHz, DMSO-d_6): δ 8.76 (d, 1H, J = 1.5 Hz), 8.74 (d, 1H, J = 1.5 Hz), 8.04 (d, 1H, J = 1.8 Hz), 8.02 (d, 1H, J = 1.8 Hz), 7.07 (s, 1H), 6.28 (s, 1H), 2.72 (s, 3H), 2.25 (s, 3H).

*2-(3,5-Dimethyl-1H-pyrazol-1-yl)-6-(pyridin-3-yl)pyrimidin-4(3H)-one (**21**).* Synthesized from intermediate **56g** following a protocol similar to compound **1**. Yield 56% (white solid). HPLC purity: 99%. LC−MS APCI: calcd for $C_{14}H_{13}N_5O$, 267.29; observed m/z $[M + H]^+$, 268.1. ^1H NMR (300 MHz, DMSO-d_6): δ 9.27 (dd, 1H, J = 3 and 1.5 Hz), 8.72 (dd, 1H, J = 6 and 3 Hz), 8.45 (dt, 1H, J = 9 and 3 Hz), 7.56 (ddd, 1H, J = 9, 6 and 1.5 Hz), 7.02 (s, 1H), 6.27 (s, 1H), 2.71 (s, 3H), 2.24 (s, 3H).

*N-(4-(2-(3,5-Dimethyl-1H-pyrazol-1-yl)-6-oxo-1,6-dihydropyrimidin-4-yl)phenyl) Methanesulfonamide (**22**).* In 1,4-dioxane (2 mL) solution of *N*-(4-(2-chloro-6-oxo-1,6-dihydropyrimidin-4-yl)phenyl)-methanesulfonamide (**69a** 0.09 g, 0.300 mmol), under a nitrogen atmosphere, cesium carbonate (0.147 g, 0.450 mmol), 3,5-Dimethylpyrazole (0.035 g, 0.360 mmol), XantPhos (0.052 g, 0.090 mmol), and Tris(dibenzylideneacetone)dipalladium(0) (0.041 g, 0.045 mmol) were added, and the mixture was heated at 130 °C for 18 h in a sealed tube. The reaction mixture was cooled to room temperature, concentrated in vacuo, filtered, and washed with DCM/MeOH, (80:20) and the filtrate concentrated to yield the crude product. The crude product was dissolved in 1 mL of water and acidified with 1 M HCl, then concentrated and purified by preparative HPLC to afford **22** as an off-white solid (3 mg, 8.01 μmol, 3% yield). HPLC purity: 96%. LC−MS APCI: calcd for $C_{16}H_{17}N_5O_3S$, 359.40; observed m/z $[M + H]^+$, 360.1. ^1H NMR (300 MHz, DMSO-d_6): δ 8.00 (d, J = 8.4 Hz, 2H), 7.27 (d, J = 8.3 Hz, 2H), 6.57 (s, 1H), 6.14 (s, 1H), 3.03 (s, 3H), 2.65 (s, 3H), 2.21 (s, 3H).

*4-(2-(3,5-Dimethyl-1H-pyrazol-1-yl)-6-oxo-3,6-dihydropyrimidin-4-yl)-N-methylbenzamide (**23**).* Synthesis protocol was the same as for compound **22**, starting from intermediate 4-(2-chloro-6-oxo-1,6-dihydropyrimidin-4-yl)-*N*-methylbenzamide (**69b**). Yield: 38% (white solid). HPLC purity: 97%; LC−MS APCI: calcd for $C_{17}H_{17}N_5O_2$, 323.128; observed m/z $[M + H]^+$, 324.1. ^1H NMR (400 MHz, DMSO-d_6): δ 8.27 (d, J = 8.5 Hz, 2H), 7.96 (d, J = 8.5 Hz, 2H), 6.67 (s, 1H), 6.18 (s, 1H), 2.80 (s, 3H), 2.73 (s, 3H), 2.20 (s, 3H).

*2-(3,5-Dimethyl-1H-pyrazol-1-yl)-6-(4-(methylsulfonyl)phenyl)-pyrimidin-4(1H)-one (**24**).* Synthesis protocol was the same as for compound **22**, starting from intermediate 2-chloro-6-(4-(methylsulfonyl)phenyl)pyrimidin-4(3H)-one (**69c**). Yield: 32% (white solid). HPLC purity: 98%; LC−MS APCI: calcd for $C_{16}H_{16}N_4O_3S$, 344.39; observed m/z $[M + H]^+$, 345.1. ^1H NMR (300 MHz, DMSO-d_6): δ 8.52−8.42 (m, 2H), 8.09 (d, J = 8.3 Hz, 2H), 6.77 (s, 1H), 6.20 (s, 1H), 3.29 (s, 3H), 2.75 (s, 3H), 2.22 (s, 3H).

*2-(3,5-Dimethyl-1H-pyrazol-1-yl)-6-(4-morpholinophenyl)-pyrimidin-4(1H)-one (**25**).* Synthesis protocol was the same as for compound **22**, starting from intermediate 2-chloro-6-(4-morpholinophenyl)pyrimidin-4(3*H*)-one (**69d**). Yield: 3% (white solid). HPLC purity: 95%; LC−MS APCI: calcd for $C_{19}H_{21}N_5O_2$, 351.41; observed m/z $[M + H]^+$, 352.1.^1H NMR (300 MHz, Methanol-d_4): δ 8.07 (d, J = 8.8 Hz, 2H), 7.09 (d, J = 8.8 Hz, 2H), 6.63 (s, 1H), 6.14 (s, 1H), 3.86 (s, 6H), 2.76 (s, 3H), 2.27 (s, 3H), 1.91 (s, 2H).

*2-(3,5-Dimethyl-1H-pyrazol-1-yl)-N-(4-fluorophenyl)-6-oxo-1,6-dihydropyrimidine-4-carboxamide (**26**).* 2-(3,5-dimethyl-1*H*-pyrazol-1-yl)-*N*-(4-fluorophenyl)-6-methoxypyrimidine-4-carboxamide **72** (40 mg, 0.117 mmol) was dissolved in dichloromethane (2 mL) under N_2 and BBr_3, 1 M in dichloromethane (0.352 mL, 0.352 mmol) was added and stirred under N_2 at room temperature for 48 h. The reaction was quenched with dilute HCl and diluted with dichloromethane. The dichloromethane layer was separated, and the aqueous layer was again extracted with dichloromethane. Organic layers were combined, washed with brine, and concentrated under vacuum. The residue was purified by column chromatography using 0−20% methanol in dichloromethane to give **26** as an off-white solid (12 mg, 0.035 mmol, 30% yield). HPLC purity: 96.5% LC−MS ESI: calcd for $C_{16}H_{14}FN_5O_2$, 327.113; observed m/z $[M + H]^+$, 328.10. ^1H NMR (300 MHz, DMSO-d_6): δ 12.80 (br s, 1H), 10.15 (br s, 1H), 7.81−7.86 (m, 2H), 7.24 (t, J = 9 Hz, 2H), 6.94 (s, 1H), 6.28 (s, 1H), 2.72 (s, 3H), (s, 3H).

*2-(3,5-Dimethyl-1H-pyrazol-1-yl)-4-(4-fluorophenyl)-6-oxo-1,6-dihydropyrimidine-5-carbonitrile (**27**).* A mixture of 4-(4-fluorophenyl)-2-hydrazinyl-6-oxo-1,6-dihydropyrimidine-5-carbonitrile **74** (50 mg, 0.204 mmol) and pentane-2,4-dione (0.025 mL, 0.245 mmol) was heated in a mixture of ethanol (0.5 mL) and acetic acid (1.5 mL) at 85 °C for 3 h. The reaction was cooled, and a yellow crystalline precipitate formed was filtered under vacuum, triturated with a small amount of ethanol, and dried to afford **27** as a light-yellow solid (37 mg, 0.120 mmol, 59% yield). HPLC purity: 95.8%. LC−MS ESI: calcd for $C_{16}H_{12}FN_5O$, 309.103; observed m/z $[M - H]^+$, 308.10. ^1H NMR (300 MHz, DMSO-d_6): δ 8.05−8.10 (m, 2H), 7.46 (t, J = 9 Hz, 2H), 6.35 (s, 1H), 2.65 (s, 3H), 2.27 (s, 3H).

*2-(3,5-Dimethyl-1H-pyrazol-1-yl)-4-(4-fluorophenyl)-6-oxo-1,6-dihydropyrimidine-5-carboxamide (**28**).* 2-(3,5-Dimethyl-1*H*-pyrazol-1-yl)-4-(4-fluorophenyl)-6-oxo-1,6-dihydropyrimidine-5-carbonitrile **27** (50 mg, 0.162 mmol) was heated with H_2SO_4 (0.5 mL, 9.38 mmol) for 2 h at 80 °C. The reaction mixture was then poured slowly on ice with vigorous stirring. A white precipitate was formed which was filtered, washed with cold water and cold ethanol, and dried to give **28** as a light-yellow solid (32 mg, 0.098 mmol, 60% yield). HPLC purity: >98% LC−MS ESI: calcd for $C_{16}H_{14}FN_5O_2$, 327.113; observed m/z $[M - H]^+$, 326.10. ^1H NMR (300 MHz, DMSO-d_6): δ 7.87−7.92 (m, 2H), 7.83 (br s, 1H), 7.50 (br s, 1H), 7.32 (t, J = 9 Hz, 2H), 6.25 (s, 1H), 2.62 (s, 3H), 2.24 (s, 3H).

*2-(3,5-Dimethyl-1H-pyrazol-1-yl)-4-(4-fluorophenyl)-6-oxo-1,6-dihydropyrimidine-5-carboxylic Acid (**29**).* In a 7 mL reaction vial, 2-(3,5-dimethyl-1*H*-pyrazol-1-yl)-4-(4-fluorophenyl)-6-oxo-1,6-dihydropyrimidine-5-carboxamide **28** (20 mg, 0.061 mmol) and *tert*-butyl nitrite (0.022 mL, 0.183 mmol) were stirred in acetic acid (0.5 mL) a 75 °C for 3 h. A white precipitate was formed. It was centrifuged out, washed with cold ethanol, and dried in an oven to give **29** as a white solid (12 mg, 0.037 mmol, 60% yield). HPLC purity: >99% LC−MS ESI: calcd for $C_{16}H_{13}FN_4O_3$, 328.097; observed m/z $[M - H]^+$, 327.10. ^1H NMR (300 MHz, DMSO-d_6): δ 7.77−7.81 (m, 2H), 7.35 (t, J = 9 Hz, 2H), 6.27 (s, 1H), 2.62 (s, 3H), 2.24 (s, 3H).

*2-(5-Ethyl-3-methyl-1H-pyrazol-1-yl)-6-(trifluoromethyl)-pyrimidin-4(3H)-one (**30**).* Synthesized from **56d** and hexane-2,4-dione following a protocol similar to compound **1**. Yield: 35% (white solid). HPLC purity: 99%. LC−MS APCI: calcd for $C_{11}H_{11}F_3N_4O$, 272.088; observed m/z $[M + H]^+$, 272.8. ^1H NMR (400 MHz, DMSO-d_6): δ 6.71 (s, 1H), 6.27 (s, 1H), 3.04 (q, J = 1.60 Hz, 2H), 2.58 (s, 1H), 2.24 (s, 2H), 1.22 (t, J = 7.20 Hz, 3H); ^{13}C NMR (100 MHz, DMSO-d_6): δ 13.22, 13.38, 13.89, 21.53, 108.02, 110.15, 110.32, 149.74, 151.87.

*2-(5-Cyclopropyl-3-methyl-1H-pyrazol-1-yl)-6-(trifluoromethyl)-pyrimidin-4(3H)-one (**31**).* Synthesized from **56d** and 1-cyclopropylbutane-1,3-dione following a protocol similar to compound **1**. Yield: 30% (white solid). HPLC purity: 98.4%. LC−MS APCI: calcd for $C_{12}H_{11}F_3N_4O$, 284.088; observed m/z $[M + H]^+$, 285.4. ^1H NMR (400 MHz, DMSO-d_6): δ 6.75 (s, 1H), 6.09 (s, 1H), 2.20 (s, 3H), 0.94−0.99 (m, 2H), 0.70−0.72 (m, 2H).

*2-(3-Methyl-5-phenyl-1H-pyrazol-1-yl)-6-(trifluoromethyl)-pyrimidin-4(3H)-one (**32**).* Synthesized from **56d** and 1-phenylbutane-1,3-dione following a protocol similar to compound **1**. Yield: 39% (white solid). HPLC purity: 98.5%. LC−MS APCI: calcd for $C_{15}H_{11}F_3N_4O$, 320.088; observed m/z $[M + H]^+$, 320.8. ^1H NMR (400 MHz, $CDCl_3$): δ 13.59 (s, 1H), 7.34−7.42 (m, 5H), 6.84 (s, 1H), 6.59 (s, 1H), 2.51 (s, 3H); ^{13}C NMR (100 MHz, DMSO-d_6): δ 13.82, 108.53, 111.52, 119.39, 121.94, 128.40, 128.81, 129.18, 130.59, 130.59, 146.20, 151.83, 153.0.

*2-(5-Amino-3-methyl-1H-pyrazol-1-yl)-6-(trifluoromethyl)-pyrimidin-4(3H)-one (**33**).* To a solution of **56d** (0.70 g, 1.28 mmol) in DMF was added 3-aminocrotonitrile (0.70 g, 8.43 mmol) and heated to 100 °C for 16 h. Water was added, extracted with ethyl acetate, and the combined organic layer was washed with saturated sodium bicarbonate solution, water, and brine solution, dried over sodium sulfate, and concentrated under vacuum. The crude product was purified by preparative HPLC to yield **33** as a white solid (0.076 g, 23%). HPLC

https://dx.doi.org/10.1021/acs.jmedchem.0c01727
J. Med. Chem. 2021, 64, 719−740

purity: 95.5%. LC−MS APCI: calcd for $C_9H_8F_3N_5O$, 259.068; observed m/z $[M + H]^+$, 259.8. ^1H NMR (400 MHz, DMSO-d_6): δ 7.15 (s, 2H), 6.30 (s, 1H), 5.23 (s, 1H), 2.08 (s, 3H). ^{13}C NMR (100 MHz, DMSO-d_6): δ 14.34, 88.68, 105.72, 120.24, 122.97, 151.14, 151.32, 151.55, 151.88, 156.03, 168.05.

*2-(5-(Ethylamino)-3-methyl-1H-pyrazol-1-yl)-6-(trifluoromethyl)-pyrimidin-4(3H)-one (**34**).* To a solution of **33** (0.20 g, 0.77 mmol), acetic acid (0.14 g, 2.30 mmol) in DMF (5 mL) and acetaldehyde (0.10 g, 2.31 mmol) were added and the reaction was allowed to stir at room temperature for 16 h. Sodium cyanoborohydride (0.24 g, 3.86 mmol) in methanol (2 mL) was added and stirred at room temperature overnight. The reaction mixture was concentrated, water was added, and extracted with ethyl acetate. The organic layer was concentrated and purified by preparative HPLC to give **34** as a white solid (0.07 g, 32%). HPLC purity: 95.2%; LC−MS APCI: calcd for $C_{11}H_{12}F_3N_5O$, 287.099; observed m/z $[M + H]^+$, 288.0. ^1H NMR (400 MHz, $CDCl_3$): δ 7.14 (s, 1H), 6.48 (s, 1H), 5.19 (s, 1H), 3.23 (q, J = 6.40 Hz, 2H), 2.19 (s, 3H), 1.32 (t, J = 7.20 Hz, 3H); ^{13}C NMR (100 MHz, CD_3OD): δ 12.56, 13.40, 39.09, 104.82, 119.62, 122.34, 152.30, 152.51, 152.85, 153.14, 155.01.

*2-(5-Ethoxy-3-methyl-1H-pyrazol-1-yl)-6-(trifluoromethyl)-pyrimidin-4(3H)-one (**35**).* To solution of sulphonyl intermediate **79** (0.50 g, 2.06 mmol) and cesium carbonate (1.6 g, 5.16 mmol) in 1,4-dioxane was added **78** (0.52 g, 4.12 mmol) in sealed tube and heated to 100 °C for 16 h. Solids were filtered through Celite and the filtrate concentrated under vacuum. The crude product was purified by preparative HPLC to afford **35** as a white solid (0.07 g, 12%). HPLC purity: 95%; LC−MS APCI: calcd for $C_{11}H_{11}F_3N_4O_2$, 288.083; observed m/z $[M + H]^+$, 288.8. ^1H NMR (400 MHz, $CDCl_3$): δ 10.43 (s, 1H), 6.53 (s, 1H), 5.80 (s, 1H), 4.28 (q, J = 7.20 Hz, 2H), 2.67 (s, 3H), 1.43 (t, J = 7.20 Hz, 3H).

*2-(5-((2-(Dimethylamino)ethyl)amino)-3-methyl-1H-pyrazol-1-yl)-6-(trifluoromethyl)pyrimidin-4(3H)-one (**36**).* To a solution of **76a** (0.10 g, 0.49 mmol) in ethanol (2.5 mL) and acetic acid (7.5 mL) was added 2-hydrazinyl-6-(trifluoromethyl)pyrimidin-4(3*H*)-one (**56d**, 0.09 g, 0.49 mmol) and heated to reflux for 5 h. The solvent was evaporated under vacuum. The crude product was purified with preparative HPLC to yield **36** as a white solid (0.06 g, 0.181 mmol, 37% yield). HPLC purity: 99.2%. LC−MS APCI: calcd for $C_{13}H_{17}F_3N_6O$, 330.142; observed m/z $[M + H]^+$, 331.0. ^1H NMR (300 MHz, DMSO-d_6): δ 7.65 (s, 1H), 6.48 (s, 1H), 5.17 (s, 1H), 3.21 (q, J = 6.00 Hz, 2H), 2.60 (t, J = 6.00 Hz, 2H), 2.31 (s, 6H), 2.19 (s, 3H).

*2-(5-((2-Hydroxyethyl)amino)-3-methyl-1H-pyrazol-1-yl)-6-(trifluoromethyl)pyrimidin-4(3H)-one (**37**).* A protocol similar to compound **36**. Yield: 16% (white solid). HPLC purity: 97.28%; LC−MS APCI: calcd for $C_{11}H_{12}F_3N_5O_2$, 303,094; observed m/z $[M + H]^+$, 304.0. ^1H NMR (400 MHz, $CDCl_3$): δ 7.45 (s, 1H), 6.68 (s, 1H), 5.44 (s, 1H), 3.58 (t, J = 5.20 Hz, 2H), 3.21 (t, J = 5.20 Hz, 2H), 2.16 (s, 3H).

*2-(5-((2-Methoxyethyl)amino)-3-methyl-1H-pyrazol-1-yl)-6-(trifluoromethyl)pyrimidin-4(3H)-one (**38**).* *Step 1:* To a −5 °C cooled solution of 4-methyleneoxetan-2-one (1.0 g, 11.90 mmol) in tetrahydrofuran (10 mL) was added 2-methoxyethylamine (0.90 g, 11.30 mmol) and stirred for 30 min. The solvent was evaporated under vacuum. The crude product was purified by column chromatography using 3−5% methanol in dichloromethane to afford *N*-(2-methoxyethyl)-3-oxobutanamide (1.2 g, 7.50 mmol, 63%). LC−MS APCI: calcd for $C_7H_{13}NO_3$, 159.19; observed m/z $[M + H]^+$, 160.2. ^1H NMR (300 MHz, DMSO-d_6): δ 8.13 (s, 1H), 3.29−3.36 (m, 4H), 3.20−3.27 (m, 5H), 2.13 (s, 3H). *Step 2:* To a solution of *N*-(2-methoxyethyl)-3-oxobutanamide (0.50 g, 3.14 mmol) in tetrahydrofuran (10 mL) was added Lawesson's reagent (1.40 g, 3.45 mmol) and stirred for 30 min at room temperature under a nitrogen atmosphere. Hydrazine **33** (0.61 g, 3.45 mmol) was added to the reaction mixture and stirred at room temperature for 24 h. The reaction was quenched with saturated sodium bicarbonate solution and extracted with ethyl acetate. The combined organic phase was washed with water and brine, dried over sodium sulfate, and concentrated under vacuum. The crude product was purified by preparative HPLC to yield **38** as a white solid (0.065 g, 0.22 mmol. 7% yield). HPLC purity: 98.9%. LC−MS APCI: calcd for $C_{12}H_{14}F_3N_5O_2$, 317.110; observed m/z $[M + H]^+$, 318.0. ^1H NMR (400 MHz, DMSO-d_6): δ 7.71 (s, 1H), 6.45 (s, 1H), 5.37 (s, 1H), 3.52 (t, J = 5.20 Hz, 2H), 3.27−3.33 (m, 5H), 2.13 (s, 3H). ^{13}C NMR (100 MHz, DMSO-d_6): δ 14.44, 44.66, 58.52, 70.51, 87.07, 106.26, 120.03, 122.75, 151.28, 152.24, 154.78, 166.47.

*2-(3-Methyl-5-((tetrahydro-2H-pyran-4-yl)amino)-1H-pyrazol-1-yl)-6-(trifluoromethyl)pyrimidin-4(3H)-one (**39**).* A protocol similar to compound **36**. Yield: 20% (white solid). HPLC purity: 97%. LC−MS APCI: calcd for $C_{14}H_{16}F_3N_5O_2$, 343.126; observed m/z $[M + H]^+$, 344.1. ^1H NMR (400 MHz, $CDCl_3$): δ 10.35 (s, 1H), 7.54 (s, 1H), 6.53 (s, 1H), 5.23 (s, 1H), 3.95−4.00 (m, 2H), 3.55−3.61 (m, 2H), 0.42−3.44 (m, 1H), 2.22 (s, 3H), 2.06−2.09 (m, 2H), 1.60−1.68 (m, 2H).

*2-(5-((4-Fluorophenyl)amino)-3-methyl-1H-pyrazol-1-yl)-6-(trifluoromethyl)pyrimidin-4(3H)-one (**40**).* In a sealed tube **33** (0.25 g, 0.96 mmol), 1-bromo-4-fluoro benzene (0.33 g, 1.92 mmol) and cesium carbonate (0.93 g, 2.88 mmol) were taken in dioxane (10 mL). The mixture was purged with nitrogen gas for 20 min. To this tris(dibenzylideneacetone)dipalladium(0) (0.079 g, 0.08 mmol) and XantPhos (0.07 g, 0.13 mmol) was added and sealed. The reaction mixture was stirred at 120 °C for 4 h. The reaction mixture filtered through Celite and filtrate was concentrated under vacuum. The crude product was purified by preparative HPLC to obtain **40** as a white solid (0.09 g, 0.51 mmol, 26% yield). HPLC purity: 95.4%; LC−MS APCI: calcd for $C_{15}H_{11}F_4N_5O$, 353.090; observed m/z $[M + H]^+$, 354.0. ^1H NMR (400 MHz, CD_3OD): δ 7.22−7.34 (m, 2H), 6.97−7.09 (m, 2H), 6.40 (s, 1H), 5.87 (s, 1H), 2.24 (s, 3H). ^{13}C NMR (400 MHz, CD_3OD): δ 14.00, 90.34, 105.40, 118.74, 121.42, 122.71, 124.14, 130.36, 138.72, 148.73, 152.72, 158.26, 160.06, 160.64, 176.68.

*2-(5-((2,4-Difluorophenyl)amino)-3-methyl-1H-pyrazol-1-yl)-6-(trifluoromethyl)pyrimidin-4(3H)-one (**41**).* A protocol similar to compound **36**. Yield: 8% (white solid). HPLC purity: 97.5%; LC−MS APCI: calcd for $C_{15}H_{10}F_5N_5O$, 371.081; observed m/z $[M + H]^+$, 372.4. ^1H NMR (400 MHz, $CDCl_3$): δ 10.46 (s, 1H), 9.81 (s, 1H), 7.31−7.34 (m, 1H), 6.92−6.99 (m, 2H), 6.58 (s, 1H), 5.81 (s, 1H), 2.27 (s, 3H).

*4-((3-Methyl-1-(6-oxo-4-(trifluoromethyl)-1,6-dihydropyrimidin-2-yl)-1H-pyrazol-5-yl)amino)benzonitrile (**42**).* Protocol similar to compound **36**. Yield 29% (white solid). HPLC purity: 99.9%; LC−MS APCI: calcd for $C_{16}H_{11}F_3N_6O$, 360.30; observed m/z $[M + H]^+$, 361.0. ^1H NMR (400 MHz, DMSO-d_6): δ 12.43 (s, 1H), 7.73 (d, J = 8.80 Hz, 2H), 7.17 (d, J = 8.80 Hz, 2H), 6.17 (s, 1H), 6.06 (s, 1H), 2.21 (s, 3H). ^{13}C NMR (100 MHz, DMSO-d_6): δ 14.46, 92.36, 101.50, 105.83, 116.12, 120.01, 123.59, 134.42, 143.47, 145.22, 149.10, 159.53, 171.58.

*N,N-Dimethyl-4-((3-Methyl-1-(6-oxo-4-(trifluoromethyl)-1,6-dihydropyrimidin-2-yl)-1H-pyrazol-5-yl)amino)benzamide (**43**).* Protocol similar to compound **36**. Yield 30% (white solid). HPLC purity: 97.9%. LC−MS APCI: calcd for $C_{18}H_{17}F_3N_6O_2$, 406.137; observed m/z $[M + H]^+$, 407.0. ^1H NMR (400 MHz, DMSO-d_6): δ 11.89 (s, 1H), 7.40 (d, J = 8.00 Hz, 2H), 7.09 (d, J = 8.00 Hz, 2H), 6.07 (s, 1H), 6.06 (s, 1H), 2.97 (s, 6H), 2.19 (s, 3H). ^{13}C NMR (100 MHz, DMSO-d_6): δ 14.47, 91.18, 115.60, 128.27, 129.59, 142.49, 144.92, 149.29, 170.44, 171.90.

*2-(3-Methyl-5-(pyridin-4-ylamino)-1H-pyrazol-1-yl)-6-(trifluoromethyl)pyrimidin-4(3H)-one (**44**).* Protocol similar to compound **36**. Yield 12% (white solid). HPLC purity 99.8%; LC−MS APCI: calcd for $C_{14}H_{11}F_3N_6O$, 336.28; observed m/z $[M + H]^+$, 337.0. ^1H NMR (400 MHz, DMSO-d_6): δ 12.29 (s, 1H), 8.33 (d, J = 6.40 Hz, 2H), 6.98 (d, J = 6.40 Hz, 2H), 6.18 (s, 1H), 6.05 (s, 1H), 5.32 (s, 1H), 2.21 (s, 3H).

*2-(3-Methyl-5-(pyridin-2-ylamino)-1H-pyrazol-1-yl)-6-(trifluoromethyl)pyrimidin-4(3H)-one (**45**).* Protocol similar to compound **36**. Yield 38% (white solid). HPLC purity: 98.2%. LC−MS APCI: calcd for $C_{14}H_{11}F_3N_6O$, 336.095; observed m/z $[M + H]^+$, 336.8. ^1H NMR (400 MHz, $CDCl_3$): δ 10.55 (s, 1H), 8.36 (d, J = 3.20 Hz, 1H), 7.64 (t, J = 7.20 Hz, 1H), 6.91−6.94 (m, 2H), 6.75 (d, J = 7.48 Hz, 1H), 6.59 (s, 1H), 2.32 (s, 3H); ^{13}C NMR (100 MHz, $CDCl_3$): δ 14.3, 96.13, 108.63, 111.78, 116.90, 137.89, 148.0, 151.95.

*2-(3-Methyl-5-((5-morpholinopyridin-2-yl)amino)-1H-pyrazol-1-yl)-6-(trifluoromethyl)pyrimidin-4(3H)-one (**46**).* A protocol similar to compound **36**. Yield 15% (white solid). HPLC purity: 99.6%. LC−MS APCI: calcd for $C_{18}H_{18}F_3N_7O_2$, 421.147; observed m/z $[M + H]^+$,

https://dx.doi.org/10.1021/acs.jmedchem.0c01727
J. Med. Chem. 2021, 64, 719−740

422.4. ^{1}H NMR (400 MHz, $CDCl_3$): δ 10.37 (s, 1H), 8.03 (s, 1H), 7.32 (s, 1H), 6.79 (s, 1H), 6.73 (d, J = 8.00 Hz, 1H), 6.57 (s, 1H), 3.91 (t, J = 4.80 Hz, 4H), 3.13 (t, J = 4.40 Hz, 4H), 2.30 (s, 3H).

*2-(5-(Ethylamino)-3-methyl-1H-pyrazol-1-yl)-6-(pyridin-3-yl)-pyrimidin-4(3H)-one (**47**).* To a solution of 2-(5-amino-3-methyl-1*H*-pyrazol-1-yl)-6-(pyridin-3-yl)pyrimidin-4(3*H*)-one (0.10 g, 0.37 mmol), acetic acid (0.07 g, 1.11 mmol) in DMF (5 mL) and acetaldehyde (0.05 g, 1.11 mmol) were added, and reaction mixture stirred at room temperature for 16 h. Sodium cyanoborohydride (0.11 g, 1.86 mmol) in methanol (2 mL) was added, and the reaction mixture stirred at room temperature overnight. The reaction mixture was concentrated, water was added, and extracted with ethyl acetate. The organic layer was concentrated and purified by preparative HPLC to give **47** as a white solid (0.03 g, 0.299 mmol, 27%). HPLC purity 97.53%; LC−MS APCI: calcd for $C_{15}H_{16}N_6O$, 296.139; observed m/z $[M + H]^+$, 297.2. ^{1}H NMR (400 MHz, CD_3OD): δ 9.42 (s, 1H), 8.77−8.82 (m, 2H), 7.82 (q, J = 5.20 Hz, 1H), 7.15 (s, 1H), 3.42 (q, J = 7.20 Hz, 2H), 2.40 (s, 3H), 1.39 (t, J = 7.20 Hz, 3H).

*2-(4-Bromo-3,5-dimethyl-1H-pyrazol-1-yl)-6-(trifluoromethyl)-pyrimidin-4(3H)-one (**48**).* To a solution of **12** (1.0 g, 3.87 mmol) in acetic acid (20 mL) was added bromine (0.24 mL, 4.65 mmol) at 20 °C and stirred at room temperature for 3 days. Water was added to the reaction mixture. Solids formed were filtered, washed with water, and dried. The crude product was purified by preparative HPLC to yield **48** as a white solid (0.3 g, 1.07 mmol, 23.0%). HPLC purity: 99.3%; LC−MS APCI: calcd for $C_{10}H_8BrF_3N_4O$, 335.983; observed m/z $[M - H]^+$, 337.0; 1H NMR (400 MHz, DMSO-d_6): δ 13.58 (s, 1H), 6.93 (s, 1H), 2.58 (s, 3H), 2.24 (s, 3H).

*2-(3,5-Dimethyl-4-(pyridin-3-yl)-1H-pyrazol-1-yl)-6-(trifluoromethyl)pyrimidin-4(3H)-one (**49**).* A solution of **48** (0.50 g, 1.48 mmol), pyridine-3-boronic acid (0.22 g, 1.78 mmol) and potassium carbonate (0.41 g, 2.96 mmol) in tetrahydrofuran/water (20/2 mL) was repeatedly purged with nitrogen. Pd(dppf)Cl_2 (0.18 g, 0.22 mmol) was added and heated at 70 °C for 16 h. The reaction mixture was cooled, water was added, and extracted with ethyl acetate. Combined organic layers were washed with water and brine solution, dried over sodium sulfate, and concentrated under vacuum. The crude product was purified by preparative HPLC to yield **49** as a white solid (0.10 g, 0.36 mmol, 20% yield). HPLC purity: 99.8%; LC−MS APCI: calcd for $C_{15}H_{12}F_3N_5O$, 335.099; observed m/z $[M - H]^+$, 336.1. ^{1}H NMR (400 MHz, $CDCl_3$): δ 400 MHz, $CDCl_3$: δ 8.68 (d, J = 4.88 Hz, 1H), 8.58 (s, 1H), 7.66 (d, J = 7.60 Hz, 1H), 7.48 (t, J = 7.28 Hz, 1H), 6.64 (s, 1H), 2.68 (s, 3H), 2.29 (s, 3H).

*2-(3,5-Dimethyl-4-morpholino-1H-pyrazol-1-yl)-6-(trifluoromethyl)pyrimidin-4(3H)-one (**50**). Step 1: 3-Bromopentane-2,4-dione (**80**)*—To a solution of acetylacetone (1.0 g, 10.0 mmol) in acetic acid (15 mL) was added bromine (1.9 g, 12.0 mmol) at 0 °C. The reaction was heated at 60 °C for 3 h. Saturated sodium bicarbonate solution was added, and the layer was separated. The combined organic layer was washed with water, dried over sodium sulfate, and concentrated under vacuum to yield **80** as a light-yellow solid (1.2 g, 67.0%). This was taken as such to the next step without further analysis. *Step 2: 3-Morpholinopentane-2,4-dione (**81**)*—To a solution of morpholine (0.58 g, 6.70 mmol) and triethylamine (1.1 g, 11.17 mmol) in dichloromethane (10 mL) was added **80** (1.0 g, 5.58 mmol) dissolved in dichloromethane (10 mL) at 0 °C. The reaction was stirred at room temperature for 2 h. Water was added, and the layers separated. The combined organic layers were washed with water, dried over sodium sulfate, and concentrated under vacuum to yield **81** (0.80 g, 78%) as viscous brown oil. LC−MS APCI: calcd for $C_9H_{15}NO_3$, 185.22; observed m/z $[M + H]^+$, 186.2. ^{1}H NMR (400 MHz, DMSO-d_6): δ 4.31 (s, 1H), 3.57−3.62 (m, 4H), 2.84 (d, J = 4.40 Hz, 2H), 2.60 (d, J = 4.80 Hz, 2H), 2.18 (s, 6H). *Step 3: 2-(3,5-Dimethyl-4-morpholino-1H-pyrazol-1-yl)-6-trifluoromethylpyrimidin-4(3H)-one (**50**)*—A solution of **81** (0.30 g, 1.62 mmol) and **56d** (0.31 g, 1.62 mmol) in ethanol/acetic acid mixture (15/5 mL) was refluxed for 16 h. The solvent was evaporated under vacuum. Crude product was purified by preparative HPLC to yield **50** (0.07 g, 13%). HPLC purity: 99.9%; LC−MS APCI: calcd for $C_{14}H_{16}F_3N_5O_2$, 343.126; observed m/z $[M + H]^+$, 344.1.^{1}H NMR (400 MHz, DMSO-d_6): δ 13.10 (s, 1H), 6.79 (s, 1H), 3.69 (d, J = 2.80 Hz, 4H), 2.96 (d, J = 3.60 Hz, 4H), 2.51 (s, 3H), 2.30 (s, 3H).

*2-(5-Amino-3-cyclopropyl-1H-pyrazol-1-yl)-6-(trifluoromethyl)-pyrimidin-4(3H)-one (**51**).* To a solution of 2-hydrazinyl-6-(trifluoromethyl)pyrimidin-4(3*H*)-one (**56d**, 0.25, 1.28 mmol) in DMF (5 mL) was added 3-cyclopropyl-3-oxopropanenitrile (0.15 g, 1.41 mmol) and heated at 130 °C in a microwave for 1 h. The reaction mixture was poured into water and extracted with ethyl acetate. The organic layer washed with plenty of water and brine solution, dried over sodium sulfate, and concentrated in vacuo. The crude mass was purified by prep HPLC to give 2-(5-amino-3-cyclopropyl-1*H*-pyrazol-1-yl)-6-(trifluoromethyl)pyrimidin-4(3*H*)-one **51** as a white solid (51 mg, 0.179 mmol, 14% yield). HPLC purity: 96%; LC−MS APCI: calcd for $C_{11}H_{10}F_3N_5O$, 285.084; observed m/z $[M + H]^+$, 286.0. ^{1}H NMR (400 MHz, $CDCl_3$): δ 6.54 (s, 1H), 5.79 (br s, 2H), 5.25 (s, 1H), 1.82 (t, J = 4.40 Hz, 1H), 1.00 (d, J = 8.00 Hz, 2H), 0.82 (d, J = 2.00 Hz, 2H).

*2-(3-((Dimethylamino)methyl)-5-methyl-1H-pyrazol-1-yl)-6-(trifluoromethyl)pyrimidin-4(3H)-one (**52**). Step 1: ethyl 2,4-dioxopentanoate*—To a solution of sodium metal (0.86 g, 37.67 mmol) dissolved in ethanol (15 mL) was added a mixture of diethyl oxalate (5.0 g, 34.24 mmol) and acetone (2.0 g, 34.24 mmol) and heated at 60 °C for 16 h. The reaction mass was concentrated under vacuum, diluted with water, and the product was extracted with ethyl acetate. The organic phase was washed with water and brine, dried over sodium sulfate, and concentrated. The crude product was then purified by column chromatography using silica gel (230−400 mesh) with 10−20% ethyl acetate in petroleum ether as an eluent to yield ethyl 2,4-dioxopentanoate as yellow oil (2.1 g, 13.93 mmol, 37%). ^{1}H NMR (300 MHz, $CDCl_3$): δ 14.40 (s, 1H), 6.39 (s, 1H), 4.37 (q, J = 7.20 Hz, 2H), 2.28 (s, 3H), 1.40 (t, J = 7.20 Hz, 3H). *Step 2: Ethyl 5-methyl-1H-pyrazole-3-carboxylate (**83**)*—To a solution of ethyl 2,4-dioxopentanoate (2.0 g, 12.65 mmol) in ethanol (10 mL) and acetic acid (20 mL) was added hydrazine hydrate (0.75 g, 15.18 mmol). The reaction mixture was heated at the reflux for 16 h. Solvents were evaporated under vacuum. Water was added, and the product was extracted with ethyl acetate. The organic layer washed with saturated sodium bicarbonate solution, water, and brine, dried over sodium sulfate, and concentrated under vacuum to afford **83** an off-white solid (1.3 g, 8.6 mmol, 68%). LC−MS APCI: calcd for $C_7H_{10}N_2O_2$, 154.17; observed m/z $[M + H]^+$, 154.8. ^{1}H NMR (400 MHz, DMSO-d_6): δ 13.15 (s, 1H), 6.46 (s, 1H), 4.25 (q, J = 7.20 Hz, 2H), 2.26 (s, 3H), 1.27 (t, J = 6.80 Hz, 3H). *Step 3: 5-methyl-1H-pyrazole-3-carbaldehyde*—To a solution of **83** (4.0 g, 25.97 mmol) in dichloromethane (50 mL) at −78 °C was added di-isobutylaluminiumhydride (1 M in dichloromethane, 52.0 mL, 51.94 mmol) dropwise under a nitrogen atmosphere. The reaction mixture was stirred at −78 °C for 2 h. It was then quenched with methanol at −78 °C, warmed to room temperature, and washed with water. The organic phase was dried over sodium sulfate and concentrated under vacuum to yield 5-methyl-1*H*-pyrazole-3-carbaldehyde. This material was taken as such for the next step without purification. *Step 4: N,N-Dimethyl-1-(5-methyl-1H-pyrazol-3-yl)-methanamine (**84**)*—To a solution of 5-methyl-1*H*-pyrazole-3-carbaldehyde (1.0 g, 9.09 mmol) in methanol was added *N*,*N*-dimethyl amine (2a M in tetrahydrofuran, 23 mL, 45.45 mmol) and stirred for 24 h at room temperature. Sodium cyanoborohydride (1.7 g, 27.27 mmol) was added to the reaction and stirred at room temperature for another 4 h. The reaction mixture was concentrated, the crude material diluted with water, and the product was extracted with ethyl acetate. The organic layer washed with water and brine solution, dried over sodium sulfate, and concentrated under vacuum to afford **84** as a white solid (0.60 g, 4.31 mmol, 48%). LC−MS APCI: calcd for $C_7H_{13}N_3$, 139.20; observed m/z $[M + H]^+$, 139.8. *Step 5: 2-(3-((Dimethylamino)methyl)-5-methyl-1H-pyrazol-1-yl)-6-(trifluoromethyl) pyrimidin-4(3H)-one (**52**)*—A solution of **84** (0.60 g, 4.31 mmol), sulfonyl intermediate **79** (0.48 g, 2.15 mmol) and cesium carbonate (2.0 g, 6.37 mmol) in 1,4-dioxane was heated in sealed tube at 130 °C for 16 h. The reaction mixture was filtered through Celite and the filtrate was concentrated under vacuum. The crude product was then purified by preparative HPLC to yield the free base as a gum. It was dissolved in dichloromethane and stirred with hydrogen chloride in 1,4-dioxane

https://dx.doi.org/10.1021/acs.jmedchem.0c01727
J. Med. Chem. 2021, 64, 719−740

(in excess) for 2 h. Solvents were evaporated under vacuum, formed solids were washed with diethyl ether, and dried under vacuum to afford **52** (0.06 g, 9.38%) as a white hydrochloride salt. HPLC purity: 99.8%. LC−MS APCI: calcd for $C_{12}H_{14}F_3N_5O$, 301.115; observed m/z $[M + H]^+$, 302.2. ^{1}H NMR (400 MHz, CD_3OD): δ 6.83 (s, 1H), 6.59 (s, 1H), 4.43 (s, 2H), 2.98 (s, 6H), 2.75 (s, 3H).

*1-(4-(4-Fluorophenyl)-6-oxo-1,6-dihydropyrimidin-2-yl)-5-methyl-1H-pyrazole-3-carboxylic Acid (**53**).* To solution of 6-(4-fluorophenyl)-2-(methylsulfonyl)pyrimidin-4(3*H*)-one (0.3 g, 1.118 mmol) **85** (Synthesized according to protocol for compound **79**) and cesium carbonate (0.911 g, 2.80 mmol) in DMF was added **83** (0.172 g, 1.118 mmol) in a sealed tube and heated to 130 °C in a microwave for 2 h. The reaction mixture was concentrated under vacuum and then was purified by preparative HPLC to yield **53** as an off-white solid (60 mg, 0.179 mmol, 16% yield). HPLC purity: 94%. LC−MS APCI: calcd for $C_{15}H_{11}FN_5O_3$, 314.27; observed m/z $[M + H]^+$, 315.1. ^{1}H NMR (300 MHz, Methanol-d_4): δ 8.19−8.08 (m, 2H), 7.26 (t, J = 8.8 Hz, 2H), 6.77 (s, 1H), 6.66 (d, J = 1.1 Hz, 1H), 2.93−2.82 (m, 3H).

*1-(4-(4-Fluorophenyl)-6-oxo-1,6-dihydropyrimidin-2-yl)-N,N,5-trimethyl-1H-pyrazole-3-carboxamide (**54**).* To a solution of HATU (0.036 g, 0.095 mmol), **53** (0.02 g, 0.064 mmol) and dimethylamine (0.017 mL, 0.191 mmol) in DMF was added triethylamine (0.018 mL, 0.127 mmol) and reaction mixture was stirred at 35 °C overnight. Upon completion, the reaction mixture was concentrated *in vacuo*, washed with 10% LiCl, and the resulting precipitate was filtered to yield **54** as a white solid (5 mg, 0.014 mmol, 22% yield). HPLC purity: 96%. LC−MS APCI: calcd for $C_{17}H_{16}FN_5O_2$, 341.34; observed m/z $[M + H]^+$, 342.1.^{1}H NMR (300 MHz, DMSO-d_6): δ 8.21 (dd, J = 8.9, 5.6 Hz, 2H), 7.37 (t, J = 8.9 Hz, 2H), 7.08 (s, 1H), 6.64 (d, J = 1.0 Hz, 1H), 3.27 (s, 3H), 3.01 (s, 3H), 2.74 (d, J = 0.9 Hz, 3H).

■ ASSOCIATED CONTENT

Supporting Information

The Supporting Information is available free of charge at https://pubs.acs.org/doi/10.1021/acs.jmedchem.0c01727.

Synthesis and analytical data of intermediates, microbiology assays, MIC data against clinical isolates, screening data against MmpL3 under-expressing strain of *Mtb*, *in vitro* DMPK assays, and mouse pharmacokinetic studies (PDF)

LCMS HPLC and NMRs of lead compounds (PDF)

Data from RNA microarray experiment (XLSX)

Data from RNA microarray experiment (XLSX)

Molecular formula strings and some data (CSV)

■ AUTHOR INFORMATION

Corresponding Authors

Kelly Chibale − *Drug Discovery and Development Centre (H3D), Department of Chemistry and South African Medical Research Council Drug Discovery and Development Research Unit, Department of Chemistry and Institute of Infectious Disease and Molecular Medicine, University of Cape Town, Rondebosch 7701, South Africa;* orcid.org/0000-0002-1327-4727; Phone: +27 21 650 2553; Email: kelly.chibale@uct.ac.za

Sandeep R. Ghorpade − *Drug Discovery and Development Centre (H3D), Department of Chemistry, University of Cape Town, Rondebosch 7701, South Africa;* orcid.org/0000-0002-9311-1572; Phone: +27 21 650 1250; Email: Sandeep.ghorpade@uct.ac.za

Authors

Candice Soares de Melo − *Drug Discovery and Development Centre (H3D), Department of Chemistry, University of Cape Town, Rondebosch 7701, South Africa*

Vinayak Singh − *Drug Discovery and Development Centre (H3D) and South African Medical Research Council Drug Discovery and Development Research Unit, Department of Chemistry and Institute of Infectious Disease and Molecular Medicine, University of Cape Town, Rondebosch 7701, South Africa;* orcid.org/0000-0001-9002-2489

†† **Alissa Myrick** − *Drug Discovery and Development Centre (H3D), University of Cape Town, Rondebosch 7701, South Africa*

Sandile B. Simelane − *Drug Discovery and Development Centre (H3D), Department of Chemistry, University of Cape Town, Rondebosch 7701, South Africa*

Dale Taylor − *Drug Discovery and Development Centre (H3D), Division of Clinical Pharmacology, Department of Medicine, University of Cape Town, Observatory 7925, South Africa*

Christel Brunschwig − *Drug Discovery and Development Centre (H3D), Division of Clinical Pharmacology, Department of Medicine, University of Cape Town, Observatory 7925, South Africa*

Nina Lawrence − *Drug Discovery and Development Centre (H3D), Division of Clinical Pharmacology, Department of Medicine, University of Cape Town, Observatory 7925, South Africa*

Dirk Schnappinger − *Department of Microbiology and Immunology, Weill Cornell Medical College, New York 10065, United States*

Curtis A. Engelhart − *Department of Microbiology and Immunology, Weill Cornell Medical College, New York 10065, United States*

Anuradha Kumar − *Infectious Disease Research Institute, Seattle, Washington 98102, United States*

Tanya Parish − *Infectious Disease Research Institute, Seattle, Washington 98102, United States;* orcid.org/0000-0001-7507-0423

Qin Su − *Genomic Technologies Section, Research Technologies Branch, National Institute of Allergy and Infectious Diseases, National Institutes of Health, Bethesda, Maryland 20892, United States*

Timothy G. Myers − *Genomic Technologies Section, Research Technologies Branch, National Institute of Allergy and Infectious Diseases, National Institutes of Health, Bethesda, Maryland 20892, United States*

Helena I. M. Boshoff − *Tuberculosis Research Section, Laboratory of Clinical Infectious Diseases, National Institute of Allergy and Infectious Diseases, National Institutes of Health, Bethesda, Maryland 20892, United States;* orcid.org/0000-0002-4333-206X

Clifton E. Barry, III − *Tuberculosis Research Section, Laboratory of Clinical Infectious Diseases, National Institute of Allergy and Infectious Diseases, National Institutes of Health, Bethesda, Maryland 20892, United States*

Frederick A. Sirgel − *South African Medical Research Council Centre for Tuberculosis Research/DST/NRF Centre of Excellence for Biomedical Tuberculosis Research, Division of Molecular Biology and Human Genetics, Faculty of Medicine and Health Science, Stellenbosch University, Tygerberg 7505, South Africa*

Paul D. van Helden − *South African Medical Research Council Centre for Tuberculosis Research/DST/NRF Centre of Excellence for Biomedical Tuberculosis Research, Division of Molecular Biology and Human Genetics, Faculty of Medicine and Health Science, Stellenbosch University, Tygerberg 7505, South Africa*

Kirsteen I. Buchanan − *Drug Discovery Unit, School of Life Sciences, University of Dundee, Dundee DD1 5EH, U.K.*
Tracy Bayliss − *Drug Discovery Unit, School of Life Sciences, University of Dundee, Dundee DD1 5EH, U.K.*
Simon R. Green − *Drug Discovery Unit, School of Life Sciences, University of Dundee, Dundee DD1 5EH, U.K.;* orcid.org/0000-0001-5054-4792
Peter C. Ray − *Drug Discovery Unit, School of Life Sciences, University of Dundee, Dundee DD1 5EH, U.K.*
Paul G. Wyatt − *Drug Discovery Unit, School of Life Sciences, University of Dundee, Dundee DD1 5EH, U.K.;* orcid.org/0000-0002-0397-245X
Gregory S. Basarab − *Drug Discovery and Development Centre (H3D), Department of Chemistry and Drug Discovery and Development Centre (H3D), Division of Clinical Pharmacology, Department of Medicine, University of Cape Town, Rondebosch 7701, South Africa;* orcid.org/0000-0001-5684-6046
Charles J. Eyermann − *Drug Discovery and Development Centre (H3D), Department of Chemistry, University of Cape Town, Rondebosch 7701, South Africa*

Complete contact information is available at: https://pubs.acs.org/10.1021/acs.jmedchem.0c01727

Author Contributions

C.S.d.M. and V.S. contributed equally to the work. Chemical synthesis, compound design, and SAR expansion were performed by C.S.d.M., S.B.S., and S.R.G. Computational and compound design support was provided by C.J.E. Iron complementation experiment and the analysis was performed by V.S. Analysis and interpretation of the biology data from target deconvolution studies was performed by V.S. and A.M. *In vivo* PK experiments including MetID studies were performed by D.T. and C.B. *In vitro* DMPK data were analyzed by N.L. The cytochrome P450 inhibition experiment was performed by N.L. Screening against MmpL3 conditional knockdown mutant was conducted by C.E. and the data were analyzed by C.E. and D.S. Screening against MmpL3 mutant strains was carried out by A.K. with data analysis by A.K. and T.P. The screening of MMV compound library and RNA microarray experiment were performed by H.I.M.B. Screening conceptualization and funding support by C.E.B. Agilent microarray protocols were developed by Q.S. and T.G.M. The synthesis of initial hits was performed by K.I.B. Data analysis and compound acquisition performed by T.B. Compound design and data analysis performed by P.C.R. data analysis and manuscript review by S.R.G.. Scientific concept and funding acquisition by P.G.W. G.S.B. provided scientific and strategic guidance for the work and edited the manuscript. Introduction and target deconvolution sections of the manuscript were written by V.S. SAR, DMPK and part of synthesis and experimental sections were written by S.R.G. Synthesis and chemistry experimental sections were written by C.S.d.M, and K.C. provided inputs on compound design, SAR analysis, and edited the manuscript. All the authors have given approval to the final version of the manuscript.

Funding

The project was funded through Global Health Grants (numbers OPP1066878 and OPP1024038) received from the Bill and Melinda Gates Foundation, the Division of Intramural Research of the NIAID/NIH and the Strategic Health Innovation Partnerships (SHIP) unit of the South African Medical Research Council (SAMRC). The University of Cape Town, SAMRC, and South African Research Chairs Initiative of the Department of Science and Technology, administered through the South African National Research Foundation are gratefully acknowledged for support (K.C.).

Notes

The authors declare no competing financial interest.
[††]AM deceased in November 2019.

■ ACKNOWLEDGMENTS

MMV, Meyrin, Switzerland for donating the compound library. Dr. Sridevi Bashayam, Dr. Jayan Joseph, Dr. Jayanth Thiruvellore, and Rajkumar Dhinakaran, Syngene, India for profound chemistry support. Ronnett Seldon from TB biology, H3D for performing MIC and biology triage assays. Dr. Nicole Cardoso from TB biology, H3D for helping in Fe-chelation experiment. Prof. Digby Warner, University of Cape Town for useful discussions on biology triage assays, Technical staff at *in vitro* DMPK and parasitology divisions of H3D for excellent technical assistance in generating all *in vitro* DMPK and cytotoxicity data, Marianna de Kock and Claudia Spies, SAMRC and Stellenbosch University, South Africa for excellent technical assistance in generating MICs against clinical TB isolates. AbbVie Incorporation, North Chicago, IL, USA for *in vitro* safety screening. Lina Castro, Shilah Bonnett and Megha Gupta from Infectious Disease Research Institute for technical assistance and support.

■ ABBREVIATIONS

AUC, area under the curve; BuOH, butanol; CS_2, carbon disulfide; DIAD, diisopropyl azodicarboxylate; DIPEA, diisopropylethylamine; DMF, *N*,*N*-dimethylformamide; EtOAc, ethyl acetate; EtOH, ethanol; fu, fraction unbound; HATU, 1-[bis(dimethylamino)methylene]-1*H*-1,2,3-triazolo[4,5-*b*]-pyridinium 3-oxid hexafluorophosphate; MIC, minimum inhibitory concentration; mCPBA, *meta*-chloroperbenzoic acid; $NaBH_4$, $NaCNBH_3$, sodium cyanoborohydride; $POCl_3$, phosphorus(V) oxychloride; RT, room temperature; SAR, structure−activity relationship; $SOCl_2$, thionyl chloride; TB, tuberculosis; THF, tetrahydrofuran

■ REFERENCES

(1) World Health Organization. *Global Tuberculosis Report*; World Health Organization: Geneva, 2019.
(2) Mabhula, A.; Singh, V. Drug-resistance in Mycobacterium tuberculosis: where we stand. *Medchemcomm* **2019**, *10*, 1342−1360.
(3) https://www.newtbdrugs.org/pipeline (accessed March 18, 2019).
(4) Soares de Melo, C.; Feng, T.-S.; van der Westhuyzen, R.; Gessner, R. K.; Street, L. J.; Morgans, G. L.; Warner, D. F.; Moosa, A.; Naran, K.; Lawrence, N.; Boshoff, H. I. M.; Barry, C. E., 3rd; Harris, C. J.; Gordon, R.; Chibale, K. Aminopyrazolo[1,5-a]pyrimidines as potential inhibitors of Mycobacterium tuberculosis: structure activity relationships and ADME characterization. *Bioorg. Med. Chem.* **2015**, *23*, 7240−7250.
(5) Wilson, C. R.; Gessner, R. K.; Moosa, A.; Seldon, R.; Warner, D. F.; Mizrahi, V.; Soares de Melo, C.; Simelane, S. B.; Nchinda, A.; Abay, E.; Taylor, D.; Njoroge, M.; Brunschwig, C.; Lawrence, N.; Boshoff, H. I. M.; Barry, C. E., 3rd; Sirgel, F. A.; van Helden, P.; Harris, C. J.; Gordon, R.; Ghidelli-Disse, S.; Pflaumer, H.; Boesche, M.; Drewes, G.; Sanz, O.; Santos, G.; Rebollo-Lopez, M. J.; Urones, B.; Selenski, C.; Lafuente-Monasterio, M. J.; Axtman, M.; Lelièvre, J.; Ballell, L.; Mueller, R.; Street, L. J.; Ghorpade, S. R.; Chibale, K. Novel antitubercular 6-dialkylaminopyrimidine carboxamides from phenotypic whole-cell high throughput screening of a softfocus library:

structure-activity relationship and target identification studies. *J. Med. Chem.* **2017**, *60*, 10118−10134.
(6) Liang, J.; Labadie, S.; Zhang, B.; Ortwine, D. F.; Patel, S.; Vinogradova, M.; Kiefer, J. R.; Mauer, T.; Gehling, V. S.; Harmange, J.-C.; Cummings, R.; Lai, T.; Liao, J.; Zheng, X.; Liu, Y.; Gustafson, A.; Van der Porten, E.; Mao, W.; Liederer, B. M.; Deshmukh, G.; An, L.; Ran, Y.; Classon, M.; Trojer, P.; Dragovich, P. S.; Murray, L. From a novel HTS hit to potent, selective, and orally bioavailable KDM5 inhibitors. *Bioorg. Med. Chem. Lett.* **2017**, *27*, 2974−2981.
(7) Dragset, M. S.; Poce, G.; Alfonso, S.; Padilla-Benavides, T.; Ioerger, T. R.; Kaneko, T.; Sacchettini, J. C.; Biava, M.; Parish, T.; Argüello, J. M.; Steigedal, M.; Rubin, E. J. A novel antimycobacterial compound acts as an intracellular iron chelator. *Antimicrob. Agents Chemother.* **2015**, *59*, 2256−2264.
(8) Hao, L.; Liu, T.; Chen, J.; Zhang, X. Bis{tris-[3-(2-pyrid-yl)-1H-pyrazole]nickel(II)} dodeca-molybdo(V,VI)phosphate hexa-hydrate. *Acta Crystallogr., Sect. E: Struct. Rep. Online* **2010**, *66*, m319−m320.
(9) Rajnák, C.; Schäfer, B.; Šalitroš, I.; Fuhr, O.; Ruben, M.; Boča, R. Influence of the charge of the complex unit on the SCO properties in pyrazolyl-pyridinyl-benzimidazole based Fe(II) complexes. *Polyhedron* **2017**, *135*, 189−194.
(10) Attaby, F. A.; Eldin, S. M. Synthesis of pyrimidine, thiazolopyrimidine, pyrimidotriazine and triazolopyrimidine derivatives and their biological evaluation. *Z. Naturforsch., B: J. Chem. Sci.* **1999**, *54*, 788−798.
(11) Tait, B. P.; Noel, A.; Cullen, M. Proteostasis Regulators for Treating Cystic Fibrosis and other Protein Misfolding Diseases. WO2012154880 A1, 2012.
(12) Burgula, L. N.; Radhakrishnan, K.; Kundu, L. M. Synthesis of modified uracil and cytosine nucleobases using a microwave-assisted method. *Tetrahedron Lett.* **2012**, *53*, 2639−2642.
(13) Zhang, Z.; Wallace, M. B.; Feng, J.; Stafford, J. A.; Skene, R. J.; Shi, L.; Lee, B.; Aertgeerts, K.; Jennings, A.; Xu, R.; Kassel, D. B.; Kaldor, S. W.; Navre, M.; Webb, D. R.; Gwaltney, S. L. Design and synthesis of pyrimidinone and pyrimidinedione inhibitors of dipeptidyl peptidase IV. *J. Med. Chem.* **2011**, *54*, 510−524.
(14) Kazimierczuk, Z.; Lipski, M.; Shugar, D. Intermediates in the synthesis of purines and pteridines: selective hydrolysis of chloropyrimidines. *Acta Biochim. Pol.* **1972**, *19*, 359−366.
(15) Peng, Z.-H.; Journet, M.; Humphrey, G. A highly regioselective amination of 6-aryl-2,4-dichloropyrimidine. *Org. Lett.* **2006**, *8*, 395−398.
(16) Cocuzza, A. J.; Hobbs, F. W.; Arnold, C. R.; Chidester, D. R.; Yarem, J. A.; Culp, S.; Fitzgerald, L.; Gilligan, P. J. 4-aryl-2-anilinopyrimidines as corticotropin-releasing hormone (CRH) antagonists. *Bioorg. Med. Chem. Lett.* **1999**, *9*, 1057−1062.
(17) Gong, Y.; Pauls, H. W. A convenient synthesis of heteroaryl benzoic acids via Suzuki reaction. *Synlett* **2000**, 829−831.
(18) Gronowitz, S.; Hornfeldt, A. B.; Kristjansson, V.; Musil, T. On the synthesis of various thienylpyrimidines and selenienylpyrimidines. *Chem. Scr.* **1986**, *26*, 305−309.
(19) Jiang, B.; Yang, C.-g. Synthesis of indolylpyrimidines via cross-coupling of indolylboronic acid with chloropyrimidines: facile synthesis of meridianin D. *Heterocycles* **2000**, *53*, 1489−1498.
(20) Schomaker, J. M.; Delia, T. J. Arylation of halogenated pyrimidines via a Suzuki coupling reaction. *J. Org. Chem.* **2001**, *66*, 7125−7128.
(21) Basavaraja, H. S.; Nagamani, J. E.; Kumar, M. M.; Padmashali, B. Antimicrobial evaluation of novel substituted pyrimidinopyrazoles and pyrimidinotriazoles. *J. Adv. Pharm. Technol. Res.* **2010**, *1*, 236−244.
(22) Patel, A.; Pasha, T. Y.; Kothari, R. Synthesis and biological evaluation of some novel heterocyclic compounds as protein tyrosine phosphatase (PTP-1B) Inhibitor. *J. Chem. Pharmaceut. Res.* **2015**, *7*, 509−517.
(23) Yedage, S. L.; Bhanage, B. M. tert-Butyl nitrite-mediated synthesis of N-nitrosoamides, carboxylic acids, benzocoumarins, and isocoumarins from amides. *J. Org. Chem.* **2017**, *82*, 5769−5781.
(24) Dodd, D. S.; Martinez, R. L. One-pot synthesis of 5-(substituted-amino)pyrazoles. *Tetrahedron Lett.* **2004**, *45*, 4265−4267.
(25) Peruncheralathan, S.; Yadav, A. K.; Ila, H.; Junjappa, H. Highly regioselective synthesis of 1-aryl-3 (or 5)-alkyl/aryl-5 (or 3)-(N-cycloamino)pyrazoles. *J. Org. Chem.* **2005**, *70*, 9644−9647.
(26) Kumar, A.; Aggarwal, V.; Ila, H.; Junjappa, H. A novel and convenient synthesis of 2-amino-4-(N-alkyl-N-arylamino)-pyrimidines using polarized ketene S,S-acetals and S,N-acetals. *Synthesis* **1980**, 748−751.
(27) Rahman, A.; Vishwakarma, J. N.; Yadav, R. D.; Ila, H.; Junjappa, H. Reaction of alpha-ketoketene S,N-acetals with hydroxylamine - a facile general-route to 5-aryl-3-(N-arylamino, N-alkylamino, or N-azacycloalkyl)-isoxazoles. *Synthesis* **1984**, 247−249.
(28) Singh, O. M.; Junjappa, H.; Ila, H. Reaction of lithioamino anions with alpha-oxoketene dithioketals: an improved and a new general method for the synthesis of alpha-oxoketene S,N- and N,N-ketals. *J. Chem. Soc., Perkin Trans. 1* **1997**, *23*, 3561−3566.
(29) Grange, J. M.; Winstanley, P. A.; Davies, P. D. O. Clinically Significant Drug Interactions with Antituberculosis Agents. *Drug Saf.* **1994**, *11*, 242−251.
(30) Sriwijitalai, W.; Wiwanitkit, V. Drug−drug interaction analysis: Antituberculosis drugs versus antiretroviral drugs. *Biomed. Biotechnol. Res. J.* **2019**, *3*, 101.
(31) Gleeson, M. P. Plasma protein binding affinity and its relationship to molecular structure: an in-silico analysis. *J. Med. Chem.* **2007**, *50*, 101−112.
(32) Lynch, J. J., III; Van Vleet, T. R.; Mittelstadt, S. W.; Blomme, E. A. G. Potential functional and pathological side effects related to off-target pharmacological activity. *J. Pharmacol. Toxicol. Methods* **2017**, *87*, 108−126.
(33) Moosa, A.; Lamprecht, D. A.; Arora, K.; Barry, C. E., 3rd; Boshoff, H. I. M.; Ioerger, T. R.; Steyn, A. J. C.; Mizrahi, V.; Warner, D. F. Susceptibility of Mycobacterium tuberculosis cytochrome bd oxidase mutants to compounds targeting the terminal respiratory oxidase, cytochrome c. *Antimicrob. Agents Chemother.* **2017**, *61*, No. e01338.
(34) Naran, K.; Moosa, A.; Barry, C. E., 3rd; Boshoff, H. I. M.; Mizrahi, V.; Warner, D. F. Bioluminescent Reporters for rapid mechanism of action assessment in tuberculosis drug discovery. *Antimicrob. Agents Chemother.* **2016**, *60*, 6748−6757.
(35) Ioerger, T. R.; O'Malley, T.; Liao, R.; Guinn, K. M.; Hickey, M. J.; Mohaideen, N.; Murphy, K. C.; Boshoff, H. I. M.; Mizrahi, V.; Rubin, E. J.; Sassetti, C. M.; Barry, C. E., 3rd; Sherman, D. R.; Parish, T.; Sacchettini, J. C. Identification of new drug targets and resistance mechanisms in Mycobacterium tuberculosis. *PLoS One* **2013**, *8*, No. e75245.
(36) Zhang, B.; Li, J.; Yang, X.; Wu, L.; Zhang, J.; Yang, Y.; Zhao, Y.; Zhang, L.; Yang, X.; Yang, X.; Cheng, X.; Liu, Z.; Jiang, B.; Jiang, H.; Guddat, L. W.; Yang, H.; Rao, Z. Crystal Structures of membrane transporter MmpL3, an anti-TB drug target. *Cell* **2019**, *176*, 636−648.
(37) Owens, C. P.; Chim, N.; Goulding, C. W. Insights on how the Mycobacterium tuberculosis heme uptake pathway can be used as a drug target. *Future Med. Chem.* **2013**, *5*, 1391−1403.
(38) Tullius, M. V.; Harmston, C. A.; Owens, C. P.; Chim, N.; Morse, R. P.; McMath, L. M.; Iniguez, A.; Kimmey, J. M.; Sawaya, M. R.; Whitelegge, J. P.; Horwitz, M. A.; Goulding, C. W. Discovery and characterization of a unique mycobacterial heme acquisition system. *Proc. Natl. Acad. Sci. U.S.A.* **2011**, *108*, 5051−5056.
(39) Cui, H.; Carrero-Lérida, J.; Silva, A. P. G.; Whittingham, J. L.; Brannigan, J. A.; Ruiz-Pérez, L. M.; Read, K. D.; Wilson, K. S.; González-Pacanowska, D.; Gilbert, I. H. Synthesis and evaluation of alpha-thymidine analogues as novel antimalarials. *J. Med. Chem.* **2012**, *55*, 10948−10957.
(40) Naik, M.; Raichurkar, A.; Bandodkar, B. S.; Varun, B. V.; Bhat, S.; Kalkhambkar, R.; Murugan, K.; Menon, R.; Bhat, J.; Paul, B.; Iyer, H.; Hussein, S.; Tucker, J. A.; Vogtherr, M.; Embrey, K. J.; McMiken, H.; Prasad, S.; Gill, A.; Ugarkar, B. G.; Venkatraman, J.; Read, J.; Panda, M. Structure guided lead generation for M. tuberculosis thymidylate kinase (Mtb TMK): discovery of 3-cyanopyridone and 1,6-naphthyridin-2-one as potent inhibitors. *J. Med. Chem.* **2015**, *58*, 753−766.
(41) Cole, S. T.; Brosch, R.; Parkhill, J.; Garnier, T.; Churcher, C.; Harris, D.; Gordon, S. V.; Eiglmeier, K.; Gas, S.; Barry, C. E., 3rd;

https://dx.doi.org/10.1021/acs.jmedchem.0c01727
J. Med. Chem. 2021, 64, 719−740

Tekaia, F.; Badcock, K.; Basham, D.; Brown, D.; Chillingworth, T.; Connor, R.; Davies, R.; Devlin, K.; Feltwell, T.; Gentles, S.; Hamlin, N.; Holroyd, S.; Hornsby, T.; Jagels, K.; Krogh, A.; McLean, J.; Moule, S.; Murphy, L.; Oliver, K.; Osborne, J.; Quail, M. A.; Rajandream, M.-A.; Rogers, J.; Rutter, S.; Seeger, K.; Skelton, J.; Squares, R.; Squares, S.; Sulston, J. E.; Taylor, K.; Whitehead, S.; Barrell, B. G. Deciphering the biology of Mycobacterium tuberculosis from the complete genome sequence. *Nature* **1998**, *393*, 537−544.

(42) DeJesus, M. A.; Gerrick, E. R.; Xu, W.; Park, S. W.; Long, J. E.; Boutte, C. C.; Rubin, E. J.; Schnappinger, D.; Ehrt, S.; Fortune, S. M.; Sassetti, C. M.; Ioerger, T. R. Comprehensive essentiality analysis of the Mycobacterium tuberculosis genome via saturating transposon mutagenesis. *mBio* **2017**, *8*, No. e02133.

(43) Griffin, J. E.; Gawronski, J. D.; Dejesus, M. A.; Ioerger, T. R.; Akerley, B. J.; Sassetti, C. M. High-resolution phenotypic profiling defines genes essential for mycobacterial growth and cholesterol catabolism. *PLoS Pathog.* **2011**, *7*, No. e1002251.

(44) Sassetti, C. M.; Boyd, D. H.; Rubin, E. J. Genes required for mycobacterial growth defined by high density mutagenesis. *Mol. Microbiol.* **2003**, *48*, 77−84.

(45) Serafini, A.; Boldrin, F.; Palú, G.; Manganelli, R. Characterization of a Mycobacterium tuberculosis ESX-3 conditional mutant: essentiality and rescue by iron and zinc. *J. Bacteriol.* **2009**, *191*, 6340−6344.

(46) Serafini, A.; Pisu, D.; Palù, G.; Rodriguez, G. M.; Manganelli, R. The ESX-3 secretion system is necessary for iron and zinc homeostasis in Mycobacterium tuberculosis. *PLoS One* **2013**, *8*, No. e78351.

(47) Siegrist, M. S.; Steigedal, M.; Ahmad, R.; Mehra, A.; Dragset, M. S.; Schuster, B. M.; Philips, J. A.; Carr, S. A.; Rubin, E. J. Mycobacterial Esx-3 requires multiple components for iron acquisition. *mBio* **2014**, *5*, No. e01073.

(48) Siegrist, M. S.; Unnikrishnan, M.; McConnell, M. J.; Borowsky, M.; Cheng, T.-Y.; Siddiqi, N.; Fortune, S. M.; Moody, D. B.; Rubin, E. J. Mycobacterial Esx-3 is required for mycobactin-mediated iron acquisition. *Proc. Natl. Acad. Sci. U.S.A.* **2009**, *106*, 18792−18797.

(49) Rodriguez, G. M.; Voskuil, M. I.; Gold, B.; Schoolnik, G. K.; Smith, I. ideR, An essential gene in mycobacterium tuberculosis: role of IdeR in iron-dependent gene expression, iron metabolism, and oxidative stress response. *Infect. Immun.* **2002**, *70*, 3371−3381.

(50) Kurthkoti, K.; Amin, H.; Marakalala, M. J.; Ghanny, S.; Subbian, S.; Sakatos, A.; Livny, J.; Fortune, S. M.; Berney, M.; Rodriguez, G. M. The capacity of Mycobacterium tuberculosis To survive iron starvation might enable it to persist in iron-deprived microenvironments of human granulomas. *mBio* **2017**, *8*, No. e01092.

(51) Singh, V.; Brecik, M.; Mukherjee, R.; Evans, J. C.; Svetlíková, Z.; Blaško, J.; Surade, S.; Blackburn, J.; Warner, D. F.; Mikušová, K.; Mizrahi, V. The complex mechanism of antimycobacterial action of 5-fluorouracil. *Chem. Biol.* **2015**, *22*, 63−75.

(52) Singh, V.; Donini, S.; Pacitto, A.; Sala, C.; Hartkoorn, R. C.; Dhar, N.; Keri, G.; Ascher, D. B.; Mondésert, G.; Vocat, A.; Lupien, A.; Sommer, R.; Vermet, H.; Lagrange, S.; Buechler, J.; Warner, D. F.; McKinney, J. D.; Pato, J.; Cole, S. T.; Blundell, T. L.; Rizzi, M.; Mizrahi, V. The inosine monophosphate dehydrogenase, GuaB2, is a vulnerable new bactericidal drug target for tuberculosis. *ACS Infect. Dis.* **2017**, *3*, 5−17.

(53) Ollinger, J.; Bailey, M. A.; Moraski, G. C.; Casey, A.; Florio, S.; Alling, T.; Miller, M. J.; Parish, T. A dual read-out assay to evaluate the potency of compounds active against Mycobacterium tuberculosis. *PLoS One* **2013**, *8*, No. e60531.

(54) Boshoff, H. I. M.; Myers, T. G.; Copp, B. R.; McNeil, M. R.; Wilson, M. A.; Barry, C. E. The transcriptional responses of Mycobacterium tuberculosis to inhibitors of metabolism novel insights into drug mechanisms of action. *J. Biol. Chem.* **2004**, *279*, 40174−40184.

https://dx.doi.org/10.1021/acs.jmedchem.0c01727
J. Med. Chem. 2021, 64, 719−740